UNIVERSITY OF CALIFORNIA,
IRVINE

Investigation of Nitrogenase Variants

DISSERTATION

submitted in partial satisfaction of the requirements
for the degree of

DOCTOR OF PHILOSOPHY

in Chemistry

by

Megan Paige Newcomb

Dissertation Committee:
Professor Markus Ribbe, Chair
Professor Ann Marie Carlton
Professor Jenny Yang

2019

Dedication

This dissertation is dedicated to my mother,
JoAnn Newcomb,
for her love and support.

Table of Contents

List of Figures and Tables

List of Abbreviations

A. vinelandii (Av)	*Azotobacter vinelandii*
C_2H_2	Acetylene
C_2H_4	Ethylene
C_2H_6	Ethane
C_3H_6	Propene
C_3H_8	Propane
C_4H_{10}	Butane
C_4H_8	Butene
CH_4	Methane
CO	Carbon monoxide
CO_2	Carbon dioxide
DMF	Dimethylformamide
DT	Dithionite
e^-	Electron
E. coli	*Escherichia coli*
EPR	Electron paramagnetic resonance
Eu^{II}-DTPA	Europium (II) diethylenetriaminepentaacetic acid
FID	Flame ionization detector
GC	Gas chromatography
GC-MS	Gas chromatography mass spectrometry
H^+	Proton
hr	Hour
ICP-OES	Inductively coupled plasma optical emission spectroscopy
kDa	kiloDalton
L	Liter
mM	Millimolar
M	Molar
M-cluster	Iron molybdenum cofactor
MgADP	Magnesium adenosine diphosphate
MgATP	Magnesium adenosine triphosphate
min	Minute
Mo-nitrogenase	Molybdenum nitrogenase
NMF	N-methylformamide
OD_λ	Optical density at a particular wavelength
P_i	Inorganic phosphate
RGD	Reducing gas detector

rpm	Rotations per minute
SDS-PAGE	Sodium dodecyl sulfate polyacrylamide gel electrophoresis
SmI_2	Samarium (II) iodide
Tris	Tris-(hydroxymethyl)-amino methane
UV/Vis	Ultraviolet-visible
V-cluster	Iron vanadium cofactor

Acknowledgements

I would like to thank Professor Markus Ribbe, who served as my research advisor during my time at UC Irvine. I would like to thank Professor Ribbe for his financial support and the array of lessons he has taught me. I would also like to thank Professor Yilin Hu for providing the opportunity to collaborate with her and members of her laboratory. Professors Ribbe and Hu have an infectious passion for research that was crucial for my progress and development.

This work was funded by the Department of Energy (DOE) BES grants DE-SC0016510 and DE-SC0014470 and the University of California, Irvine. I would like to thank the American Society for Microbiology for permission to include copyrighted material in Chapter 2 of this thesis and John Wiley and Sons for permission to include copyrighted material in Chapters 3 and 5 of this work.

I would like to thank my dissertation committee members, Professor Jenny Yang and Professor Ann Marie Carlton, for serving as mentors and role models for me. There are many other UC Irvine professors who have also mentored and inspired me during my time here. I would like to thank Professor Kieron Burke, Professor Jennifer Prescher, and Professor Sergey Nizkorodov for their support and wise words. I would like to thank the members of my advancement committee: Professor Jennifer Prescher, Professor Donald Blake, Professor Tom Poulos, Professor David Mobley, and Professor John Fruehauf.

I would like to thank my undergraduate advisor and mentor, Professor Alison Fisher, for teaching me to love chemistry and to see it in the world around me. I

mirrored your teaching style when working with undergraduate students, and I aimed to inspire them in the same way you inspired me.

Thank you to everyone who has helped with Science Saturday events over the years. You helped to inspire future scientists and I am incredibly grateful for your commitment and passion.

Thank you to my past and present coworkers in the Ribbe and Hu labs. Thank you for making me laugh and keeping me grounded. I am especially grateful for Dr. Nathaniel Sickerman, who patiently worked with me during my early days in the lab. Special thanks are due to Dr. Johannes Rebelein, Dr. Kazuki Tanifuji, Dr. Andrew Jasniewski, Dr. Caleb Hiller, Lee Rettberg, and Jasper Liedtke for their help and friendship. I would like to thank Dr. Kazuki Tanifuji, Dr. Andrew Jasniewski, Dr. Martin Stiebritz, Lee Rettberg, and Jasper Liedtke for helping me prepare my dissertation document and defense presentation.

Thank you to my friends. It has been an incredible pleasure to learn with and from you over the years. I would especially like to thank Jasper Liedtke for his partnership and support.

Lastly, I would like to thank my mother, JoAnn Newcomb. Thank you for working so hard to give me every available opportunity. Thank you for teaching me to be resilient. I owe you everything.

Curriculum vitae

Megan Paige Newcomb

Education

PhD in Chemistry | University of California, Irvine *December 2019*
Research in nitrogenase biochemistry and bacterial fermentation

MS in Chemistry | University of California, Irvine *June 2019*
Coursework in organic chemistry, inorganic chemistry, biochemistry, biophysics, and ecology

BA in Biochemistry | Willamette University *May 2014*
Coursework in physical chemistry, analytical chemistry, inorganic chemistry, and biochemistry

Research experience

Research Assistant | UC Irvine Chemistry Department *2015 - 2019*
Advisor: Dr. Markus Ribbe

Research Assistant | Willamette University Chemistry Department *2012 - 2014*
Advisor: Dr. Alison Fisher

Teaching experience

Teaching Assistant | UC Irvine Chemistry Department *2015 - 2019*
Courses: Organic Chemistry (51LC), Chemical Biology (128L), Honors Chemistry for non-major students (H90), and Introductory Chemistry (M2A)

Teaching Assistant |Willamette University Chemistry Department *2013*

Leadership experience

Departmental Ambassador | UC Irvine Science in Action Program *2018 - 2019*

Founder and Coordinator | Science Saturdays Outreach Program *2016 - 2019*

Vice President and Member | ΙΣΠ Women in Chemistry Honor Society *2016 - 2019*

Educational Intern | The Butterfly Conservatory, Costa Rica *2014 - 2015*

Green Fund Founder and Senator | Willamette University Senate *2010 - 2014*

Awards

Outstanding Contribution to the Department | UC Irvine Chemistry Department *May 2019*

Best Elevator Pitch | UC Irvine GPS-BIOMED Program *December 2018*

Best Biology Presentation | UC Irvine Graduate Student Research Symposium *April 2018*

Best Poster Presentation | UC Irvine Biochemistry Departmental Retreat *March 2018*

Grad Slam Champion | UC Irvine Graduate Division *March 2017*

Publications

Newcomb, M.; Lee, C. C.; Jasniewski, A.; Tanifuji, K.; Liedtke, J.; Hu, Y.; Ribbe, M. W. Characterization of a V-nitrogenase variant from *A. vinelandii* that contains a citrate-substituted cofactor. *ChemBioChem* (accepted)

Lydon, B.; Lee, C.; Tanifuji, K.; Sickerman, N.; **Newcomb, M.**; Hu, Y.; Ribbe, M. W.; Yang, J. Electrochemical characterization of isolated nitrogenase cofactors from *A. vinelandii.* *ChemBioChem* **2019** (in press)

Rebelein J. G.*; Lee, C.*; **Newcomb, M.*;** Hu, Y.; and Ribbe, M. W. Characterization of an M-Cluster-Substituted Nitrogenase VFe Protein. *mBio* **2018**, *9* (2) 310-318. *shared first-authorship

Lee, C.; Tanifuji, K.; **Newcomb, M.**; Liedtke, J.; Hu, Y.; and Ribbe, M. W. A Comparative Analysis of the CO-Reducing Activities of MoFe Proteins Containing the Mo- and V-Nitrogenase Cofactors. *ChemBioChem* **2018**, *19* (7) 649-653.

Abstract of the Dissertation

Investigations of Nitrogenase Variants

By

Megan Paige Newcomb

Doctor of Philosophy in Chemistry

University of California, Irvine, 2019

Professor Markus Ribbe, Chair

Nitrogenases are complex metalloenzymes that catalyze the reduction of nitrogen gas (N_2) to form bioavailable ammonia (NH_3) under ambient conditions. These enzymes can also reduce carbon monoxide (CO), a potent pollutant gas, into small hydrocarbon products. The molybdenum (Mo) and vanadium (V) nitrogenases are two homologous members of the nitrogenase family that are both comprised of a multi-subunit protein scaffold and a complex active site metallocofactor made up of an iron-sulfur core and an organic ligand.

The Mo- and V-nitrogenases demonstrate different capabilities with respect to the reduction of N_2 and CO. Specifically, the Mo-nitrogenase is about twice as active as V-nitrogenase at producing NH_3 from N_2. Interestingly, the V-nitrogenase is ~600-fold more active than the Mo-nitrogenase in reducing CO to hydrocarbon products. These reactivity differences likely stem from dissimilarities in the protein scaffolds and active site cofactor properties of the Mo- and V-nitrogenase variants, and the work described in this dissertation probes the roles of these aspects through biochemical and spectroscopic characterization.

A hybrid protein made up of the V-nitrogenase protein scaffold and the Mo-nitrogenase cofactor was created *in vivo* through the manipulation of bacterial growth conditions. The substrate reduction activity of the purified hybrid protein indicates that the protein scaffold of V-nitrogenase is the primary contributor to the observed differences in its CO-reducing capabilities. Additional work was conducted with a mutant of V-nitrogenase that produced an active site cofactor with an alternative organic ligand. The modified V-nitrogenase and its isolated cofactor demonstrated an increased production of NH_3 from N_2, which indicates that the organic ligand plays an important role in protonation of various small molecule substrates. The results of this work highlight the importance of the V-nitrogenase protein scaffold and its organic ligand in the production of hydrocarbon products from CO and NH_3 from N_2.

Chapter 1:

Introduction

1.1 Nitrogen fixation

Nitrogen (N) is an essential element for life and is found in vital biomacromolecules such as deoxyribonucleic acid (DNA), ribonucleic acid (RNA), and proteins. The most abundant form of nitrogen on Earth is gaseous dinitrogen (N_2), which makes up 78% of the atmosphere.[1] N_2 contains a strong triple bond and is relatively inert. Therefore, N_2 must be converted into a bioavailable form to be utilized for incorporation in biomacromolecules.[2] One important bioavailable form of nitrogen is ammonia (NH_3), which can be produced through both industrial and biological processes. Industrially, ammonia is synthesized from N_2 through the Haber-Bosch process, which requires extreme pressures and temperatures to facilitate this difficult conversion. The ammonia produced by the Haber-Bosch process is used for fertilizer and is crucial for supporting global agricultural demands. Due to the energetic requirements of the Haber-Bosch process, industrial NH_3 production accounts for an estimated 2% of global annual energy consumption.[2]

Biological systems can also convert inert N_2 into bioavailable ammonia. Diazotrophic bacteria contain nitrogenase enzymes that can reduce N_2 into two equivalents of NH_3 and one equivalent of H_2 (Reaction 1.1).[3] Unlike the Haber-Bosch process, these systems operate under ambient temperatures and pressures.

$$N_2 + 8H^+ + 16MgATP + 8e^- \rightarrow 2NH_3 + H_2 + 16MgADP + 16P_i \quad (1.1)$$

This reaction requires the input of protons (H^+), magnesium adenosine triphosphate (MgATP), and electrons (e^-). In the process of converting N_2 into NH_3, protons are both bound to N and converted into H_2. MgATP is hydrolyzed to form

magnesium adenosine diphosphate (MgADP), which produces inorganic phosphate (P_i) as a byproduct.[4,5] This ATP-dependent system requires the cooperation of multiple protein components and metallocofactors.[3,6] Biological nitrogen fixation is a topic of active research, and one research goal is to completely understand the biochemistry that allows nitrogenase to reduce N_2 under ambient conditions. A better understanding of biological nitrogen fixation could help to improve these natural processes and decrease the energetic costs of industrial ammonia production. Interestingly, nitrogenases have also been found to reduce other gaseous substrates such as carbon monoxide (CO) and carbon dioxide (CO_2). Nitrogenases convert these gases into small hydrocarbon fuel products ($C_{1\text{-}4}$ alkanes and alkenes), and the discovery of this capability launched studies of nitrogenase-based systems for converting pollutant and greenhouse gases into useful fuel products.[7–10] Nitrogenase research aims to understand the enzymatic machinery and biochemistry of substrate reduction by nitrogenase enzymes from model organisms.

Three nitrogenase variants have been discovered within diazotrophic bacteria, and each variant is identified by the transition metal contained within the respective catalytic metallocofactors: the molybdenum-containing nitrogenase (Mo-nitrogenase), the vanadium-containing nitrogenase (V-nitrogenase), and the iron-only nitrogenase (Fe-nitrogenase).[11] All three variants can reduce N_2 to NH_3 but demonstrate different catalytic efficiencies and turnover rates.[11,12] The efficacy of the variants in regard to N_2 reduction follows the trend Mo-nitrogenase > V-nitrogenase > Fe-nitrogenase, which also reflects the extent of the available characterization information for these systems.[11] These variants also demonstrate reactivity differences with other substrates. For example, in terms of converting CO into small hydrocarbons, V-nitrogenase produces longer

hydrocarbon products at a faster rate than Mo-nitrogenase. The reasons behind these discrepancies are not well-understood, and the research described in this thesis will focus on the Mo- and V-nitrogenase variants and the biochemical differences between them.

1.2 Molybdenum nitrogenase structure

Significant insight into the structure and function of nitrogenase comes from studies of the Mo-nitrogenase from the model organism *Azotobacter vinelandii* (*A. vinelandii*), a facultative anaerobe common in many soils.[3,4] Nitrogenase activity requires both reductase and catalytic protein components to facilitate a series of electron transfer events through multiple metal cofactors. For Mo-nitrogenase, these proteins are encoded by the *nif* gene cluster. The reductase component NifH (Fe protein, encoded by *nifH*) is a ~64 kDa homodimer that coordinates a redox-active [Fe_4S_4] cubic cofactor (Figure 1.1A) at the dimer interface.[14,15] NifH plays multiple roles in both biosynthesis of the catalytic M-cluster ([(*R*)-homocitrate $MoFe_7S_9C$], Figure 1.1A) and reductive catalysis. During biosynthesis of the M-cluster, NifH provides (*R*)-homocitrate and a molybdenum source.[16]

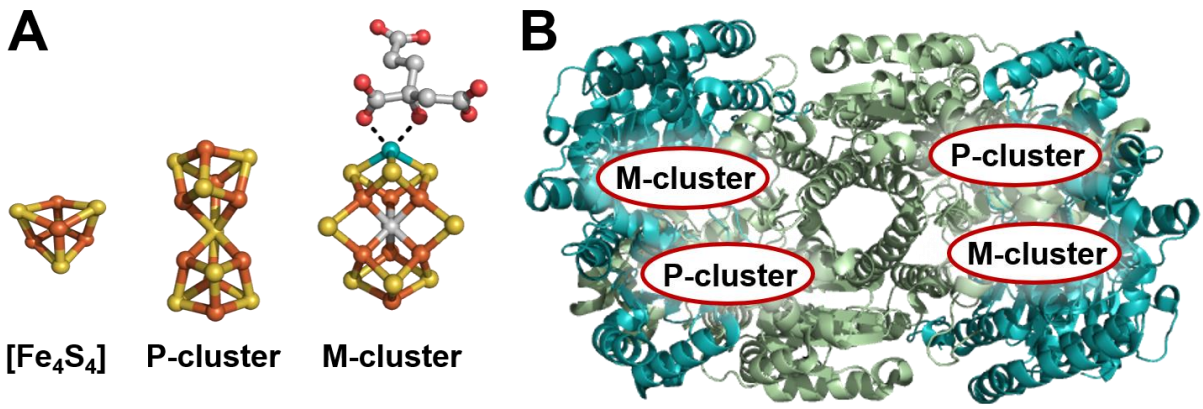

Figure 1.1: Cofactors and protein structure of Mo-nitrogenase. **A**) Cofactors of NifH and NifDK. Color codes: yellow, sulfur; orange, iron; gray, carbon; red, oxygen; teal, molybdenum. **B**) Protein structure of NifDK (D, teal; K, green). From PDB 1M34 and 1N2C.

NifH also binds and hydrolyzes ATP such that electron transfer into NifDK can occur, and its [Fe_4S_4] is crucial for electron transfer during catalysis.[17]

The catalytic component NifDK (encoded by *nifDK*) is a ~240 kDa $\alpha_2\beta_2$ heterotetramer that houses a [Fe_8S_7] P-cluster at each $\alpha\beta$ dimer interface and a catalytic M-cluster within each α subunit (Figure 1.1B). The P-cluster (Figure 1.1) is ligated at the $\alpha\beta$ interface by six cysteine residues while the M-cluster is bound within the α subunit by one cysteine and one histidine residue. The M-cluster contains a molybdenum atom within its [$MoFe_7S_9C$]-core (Figure 1.1) and can be described as two subclusters ([Fe_4S_3] and [$MoFe_3S_3$]) that are bridged by three μ_2-sulfides and one μ_6-interstitial carbide.[13,18–20] A molecule of (*R*)-homocitrate is coordinated to the molybdenum atom by the oxygen atoms of the central carboxylic acid and alcohol moiteies.[20,21] (*R*)-homocitrate is produced by the homocitrate synthase NifV, and although the role of this organic ligand is not completely understood, its presence is required for enzymatic activity.[22–25] As discussed in Chapter 3, changing the identity of the organic ligand can significantly alter nitrogenase reactivity.[21,26,27]

1.3 M-cluster biosynthesis

Biosynthesis of the catalytic M-cluster is complex and involves a series of contributing proteins. The M-cluster is synthesized outside of the catalytic protein scaffold (NifDK). In summary, the M-cluster is formed from two [Fe_4S_4] cofactors through formation of an Fe-only analog of the M-cluster (Figure 1.2A).[13,16,20,28,29] Each of these conversions occurs on different protein scaffolds as shown in Figure 1.2B.

The first step of cofactor biosynthesis begins on the NifB protein, where two [Fe_4S_4] cofactors are combined through cleavage of S-adenosylmethionine (SAM). This process is facilitated by the cleavage of SAM on a third [Fe_4S_4] cluster present within NifB, which leads to the introduction of a central carbide into the cofactor core to afford the Fe-only analog of the M-cluster ([Fe_8S_9C], L-cluster).[28–33] The L-cluster is then transferred to the scaffold protein NifEN, which is homologous to NifDK. In the presence of NifH, MgATP, and a reductant, a terminal iron atom of the NifEN-bound L-cluster is substituted for a molybdenum atom with the introduction of (*R*)-homocitrate, leading to the complete [(*R*)-homocitrate $MoFe_7S_9C$] M-cluster.[16] Once complete, the matured M-cluster is transferred

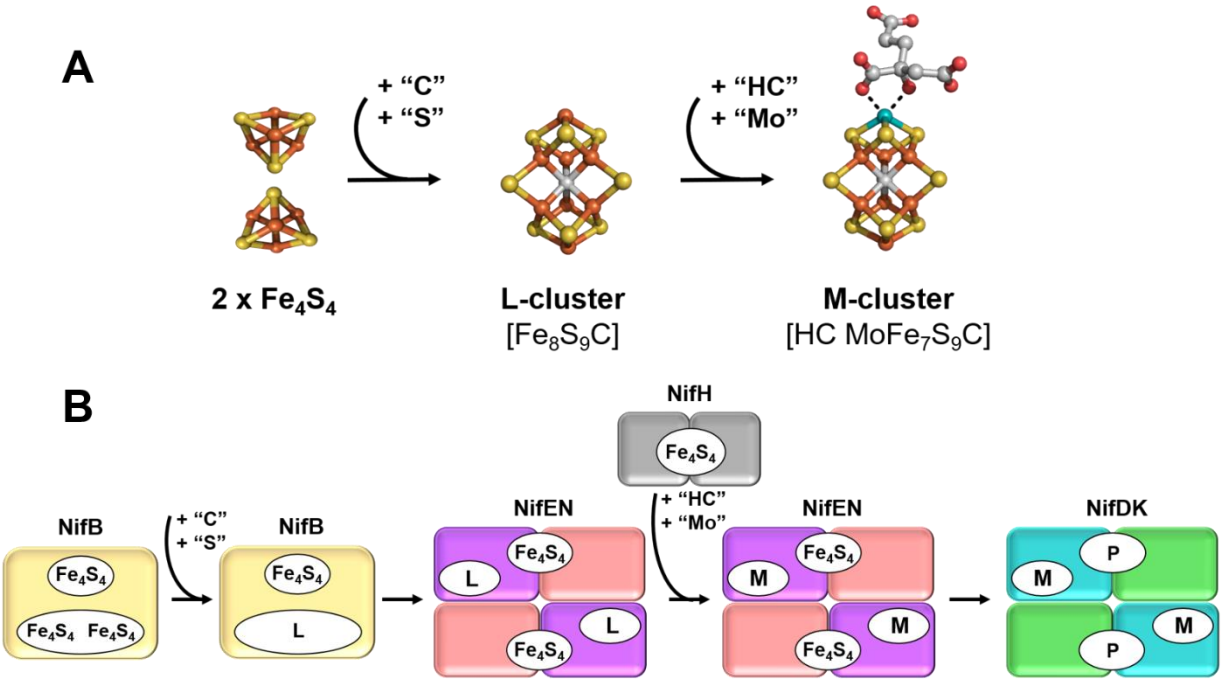

Figure 1.2: M-cluster biosynthesis. **A**) The transformation of cofactors to afford the M-cluster. The M-cluster is synthesized from two [Fe_4S_4] cofactors through formation of the L-cluster, an Fe-only analog of the M-cluster. **B**) The protein components involved in M-cluster biosynthesis. The L-cluster is synthesized on NifB prior to transfer onto NifEN. The L-cluster is matured to the M-cluster by addition of molybdenum (Mo) and (*R*)-homocitrate (HC) by NifH. Finally, the M-clusters are transferred to the active sites of NifDK.

to the active sites within NifDK (Figure 1.2B) and becomes competent for substrate reduction.[13,20,28,29]

1.4 Electron transfer and catalysis

Electron transfer is required for reduction of various substrates by nitrogenase. Electron transfer towards the M-cluster active site begins with reduction of the [Fe_4S_4] cofactor of NifH. *In vivo*, the reduction of the [Fe_4S_4] cofactor on NifH is facilitated by physiological partners such as ferredoxin and flavodoxin proteins.[34] NifH binds two molecules of ATP, which are hydrolyzed to ADP upon electron transfer. NifH can bind to either side of NifDK (Figure 1.3), and nucleotide binding causes a conformational change of the NifH-bound [Fe_4S_4] cluster.[14,35–37] Once bound to NifDK, electrons are initially transferred from NifH to the [Fe_8S_7] P-cluster and then to the catalytic M-cluster, where substrate reduction occurs (Figure 1.3).[38,14]

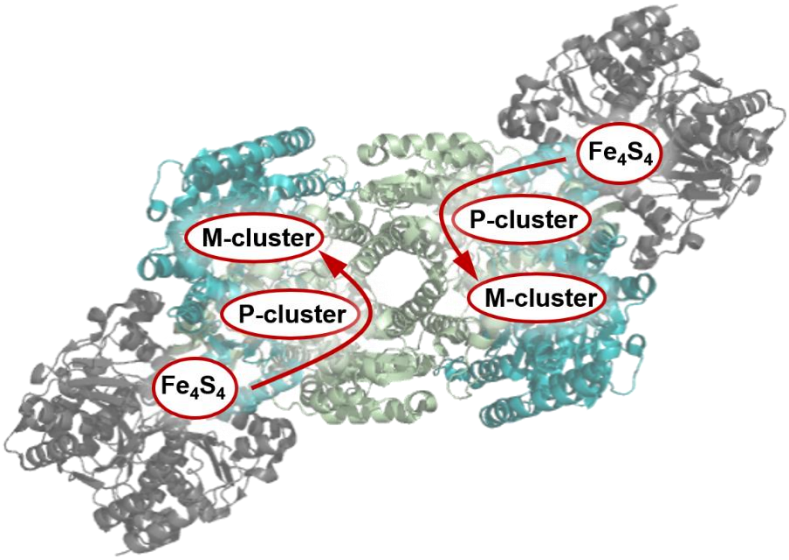

Figure 1.3: Electron transfer through Mo-nitrogenase. NifH (gray) and NifDK (K, green; D, teal). From PDB 1M34.

The reduction of N_2 into two molecules of NH_3 and one molecule of H_2 requires the transfer of eight electrons from the [Fe_4S_4] cofactor of NifH to the M-cluster of NifDK. As two molecules of ATP are required for each electron transfer, sixteen molecules of ATP

are hydrolyzed during the complete reduction of one equivalent of N_2. Eight protons are required and incorporated into the reaction products (Reaction 1.1).[3,39] The required protons are thought to be transferred as water molecules from the protein surface towards the active site. This transfer may occur through two residue-assisted proton shuttling pathways. (*R*)-homocitrate is thought to play an important role in this process, and this will be discussed further in Chapter 3.[40]

The mechanism of substrate reduction by nitrogenase is an area of active research and discussion. One interesting hypothesis for nitrogenase catalysis involves replacement of at least one of the belt-sulfur atoms (μ_2-sulfides) of the active site cofactor by substrate molecules.[41–43] Crystal structures of Mo-nitrogenase during inhibition by CO indicate that CO replaces one of the bridging sulfur atoms upon interaction with the M-cluster. This perturbation of the active site cofactor is reversible, and loss of the bound CO leads to a regeneration of the complete and active cofactor.[41] Similarly, kinetic and crystallographic studies utilizing $SeCN^-$ as an inhibitor indicated that Se could replace the same belt-sulfur atom replaced during CO inhibition. During catalysis, the Se atom replaced other adjacent belt-sulfur atoms. Putting the protein under substrate-reducing conditions led to loss of Se and regeneration of a whole and active M-cluster.[42] These studies indicated that small molecule binding may involve the temporary displacement of at least one belt-sulfur atom, providing valuable insights into the potential behavior of substrates during turnover by nitrogenase.

1.5 Vanadium nitrogenase structure and catalysis

The V-nitrogenase variant shares a similar overall structure with Mo-nitrogenase, with the homologous protein subunits encoded by the *vnf* gene cluster.[44–46] The catalytic

component VnfDGK is a ~270 kDa $\alpha_2\beta_2\delta_2$ heterohexamer, where the δ subunit (VnfG) is a small (13 kDa) protein with a currently unknown function (Figure 1.4A).[47] The α and β subunits of the V- and Mo-nitrogenase share 53% and 47% amino acid sequence homology.[48] As in NifDK, the α subunit contains a catalytic cofactor (V-cluster) and a P-cluster is coordinated between the α and β subunit interfaces (Figure 1.4A). The biosynthetic processes for V-cluster are not well-established but are proposed to mirror the biosynthesis of the M-cluster.[13,20] The reductase component of V-nitrogenase, VnfH, is a ~60 kDa homodimer that shares ~91% of amino acid sequence identity with NifH.[48] Although a crystal structure of VnfH bound to VnfDGK has not yet been reported, the homology of NifDK, VnfDGK, NifH, and VnfH indicates that electron transfer processes are probably similar between the two variants: transfer likely begins with the cubic [Fe_4S_4] cofactor of VnfH before transfer through the P-cluster and then to the catalytic V-cluster.

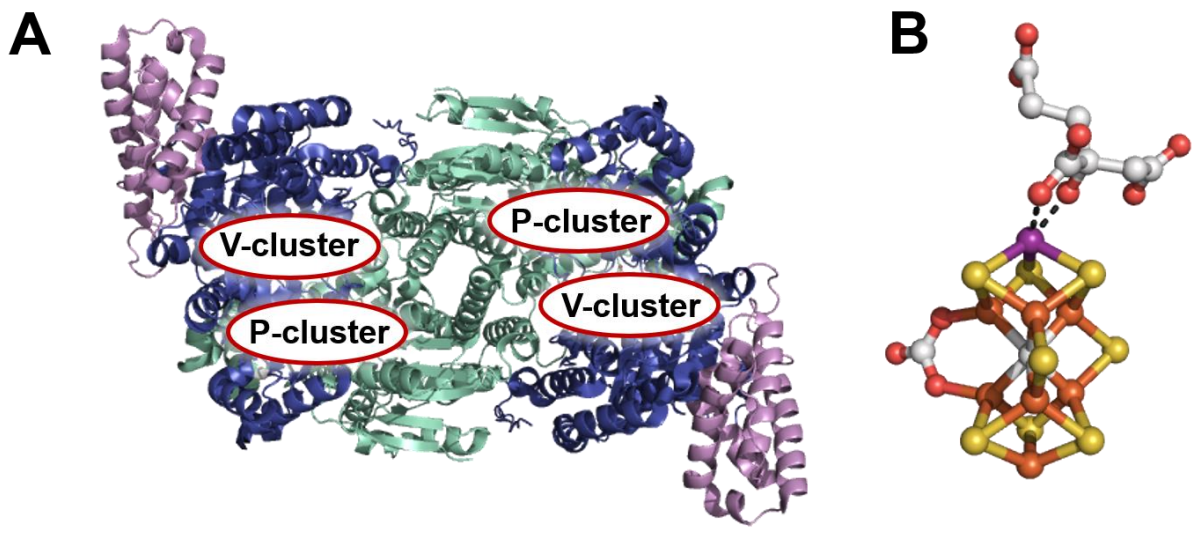

Figure 1.4: V-nitrogenase structure and cofactors. **A**) VnfDGK. Color codes: VnfD in blue, VnfK in green, and VnfG in purple. **B**) V-cluster [(*R*)-homocitrate $VFe_7S_8CCO_3$]. Color codes: purple, vanadium; yellow, sulfur; orange, iron; gray, carbon; red, oxygen. From PDB 5N6Y.

The V-cluster was previously thought to be a homolog of the M-cluster in which a vanadium atom replaced the molybdenum atom to give [(*R*)-homocitrate VFe_7S_8C]. However, a V-nitrogenase structure published in 2017 indicates that the V-cluster may contain a unique bridging ligand in place of one belt-sulfur (Figure 1.4B). Electron density maps suggest that this ligand is either a carbonate (CO_3^{2-}) or nitrate (NO_3^-) group, and subsequent calculations support the assignment as a CO_3^{2-} moiety.[47,49] This ligand is located at a different belt-sulfur site than the CO/Se binding site for Mo-nitrogenase, and further research is required to understand the potential role of this ligand in catalysis.

The first crystal structure of V-nitrogenase provided further details regarding the similarity of the V- and M-clusters. Despite the addition of an apparent carbonate or nitrate moiety, the overall geometry of both cofactors is pseudo C_3-symmetric relative to the axis that connects the Mo/V and terminal Fe atoms. Both cofactors share similar belt-sulfur distances, but the V-cluster structure is slightly elongated along the C_3 rotation axis. This elongation is primarily due to a Fe-V bond that is longer than the previously characterized Fe-Mo bond length.

An additional crystal structure of V-nitrogenase with a nitrogen-reduction reaction intermediate supports the findings of the CO and Se work conducted with Mo-nitrogenase. In this structure, a reaction intermediate, interpreted as a protonated nitrogen (N-H), replaces the same bridging sulfur as in the CO and $SeCN^-$ inhibition studies. This state seems to represent a later stage of catalysis, potentially after loss of one NH_3 molecule.[50] In the future, crystal structures that show additional binding modes and mechanistic steps will continue to elucidate the catalytic processes for V-nitrogenase.

1.6 Structural differences between Mo- and V-nitrogenase

There are multiple structural aspects that could contribute to the catalytic differences between Mo- and V-nitrogenase. At the subunit scale, the V-nitrogenase catalytic component includes an additional subunit (*δ*, VnfG) that is not observed with Mo-nitrogenase. Although research on the role of the *δ* subunit is limited, observational evidence from the research conducted for this thesis indicates that the amount of *δ* subunit present in purified V-nitrogenase samples is positively correlated with enzymatic activity. In terms of subunit interactions between the *α* and *β* subunits of VnfDGK and NifDK, each variant demonstrates different degrees of overlap and alignment of these larger subsunits.[47] These structural differences likely play a role in the catalytic differences between these two variants.

On an atomic scale, one major difference is the structures of the active site cofactors. The potential existence of a carbonate or nitrate moiety on the V-cluster may influence both the substrate-binding interactions and residue contributions to catalysis at the V-cluster.[47] Additionally, the presence of a vanadium atom in the V-cluster may influence substrate reduction due to the overall lengthened structure of the V-cluster and the resulting influence on active site and secondary sphere residue distances. Despite sharing the same organic ligand, the (*R*)-homocitrate ligand is aligned differently in the active site pockets of Mo- and V-nitrogenase.[47,50] There are multiple hypotheses for the role of the organic ligand (discussed further in Chapter 3), and the positioning of the organic ligand within the active site pocket may influence the protonation of substrates or secondary sphere amino acid interactions near the active sites of the two variants.[22,26]

1.7 Catalytic features of M- and V-nitrogenase

The reactivity of Mo- or V-nitrogenase is analyzed through activity assay experiments. Because nitrogenase cofactors are oxygen-sensitive, activity is dependent upon maintaining strictly anaerobic conditions during both purification and experimental processes. Nitrogenase enzymes purified under different conditions demonstrate altered substrate reduction capabilities. Additionally, various aspects of activity assay processes can influence overall substrate turnover. For example, increasing the ratio of reductase to catalytic proteins can increase reaction rates.

Mo- and V-nitrogenase are capable of reducing a wide variety of alternative substrates including protons (H^+), acetylene (C_2H_2), carbon monoxide (CO), and carbon dioxide (CO_2).[7–10,51–53] The work covered in this thesis utilizes N_2, H^+, C_2H_2, and CO as substrates. When supplied with the same substrate, Mo- and V-nitrogenase demonstrate different catalytic efficiencies and product distributions. For some reactions, V-nitrogenase produces products that are not observed with Mo-nitrogenase under the same conditions.[10,53] For a general comparison, selected reaction examples and associated reaction rates are included in Table 1.1 and discussed in more detail below.

Mo-nitrogenase is about twice as active as V-nitrogenase when converting N_2 into NH_3 (Reaction 1.2). V-nitrogenase also produces a smaller ratio of NH_3:H_2 compared to Mo-nitrogenase.[52] The reason behind this difference in product distribution is not completely understood, but some researchers have hypothesized that the increased production of H_2 by V-nitrogenase is a result of overall inefficiency and slower catalytic rates.[54,55]

$$N_2 + 8H^+ + 8e^- \rightarrow 2NH_3 + H_2 \qquad (1.2)$$

Nitrogenases produce H_2 from aqueous H^+, and this hydrogenase-like behavior occurs in the absence of other substrates (Reaction 1.3).[3,56] The Mo-nitrogenase is about 1.2 -fold more active than the V-nitrogenase when converting H^+ into H_2.[52]

$$2H^+ + 2e^- \rightarrow H_2 \quad (1.3)$$

The conversion of acetylene (C_2H_2) to ethylene and ethane (C_2H_4 and C_2H_6) serves as an efficient way to quantify nitrogenase activity.[8,9] Both Mo- and V-nitrogenase produce C_2H_4 from C_2H_2 (Reaction 1.4), and Mo-nitrogenase is about 3.6-fold more active than V-nitrogenase.[52] Interestingly, only the V-nitrogenase has also been shown to produce C_2H_6 from C_2H_2 (Reaction 1.5), while Mo-nitrogenase does produce C_2H_6 from C_2H_2.[52,53]

$$C_2H_2 + 2H^+ + 2e^- \rightarrow C_2H_4 \quad (1.4)$$

$$C_2H_2 + 4H^+ + 4e^- \rightarrow C_2H_6 \quad (1.5)$$

Both variants can convert CO into small hydrocarbon products. Mo-nitrogenase can form C_2 and C_3 products (alkanes and alkenes) from CO (Reaction 1.6).[10,53] V-nitrogenase is capable of making larger hydrocarbon products up to C_4H_{10} (Reaction 1.7).[10] When utilizing CO as a substrate, V-nitrogenase is ~600 times more active than the Mo-nitrogenase relative to reaction rates and the chain length of hydrocarbon products.[10,53,57] The exact stoichiometry of both reactions in terms of equivalents of substrate (x), protons (y), and electrons (z) is unknown, and the product distributions (n) vary depending upon reaction conditions.

$$x\,CO + y\,H^+ + z\,e^- \rightarrow n\,[C_2H_4 + C_2H_6 + C_3H_6 + C_3H_8] \quad (1.6)$$

$$x\,CO + x\,H^+ + z\,e^- \rightarrow n\,[CH_4 + C_2H_4 + C_2H_6 + C_3H_6 + C_3H_8 + C_4H_8 + C_4H_{10}] \quad (1.7)$$

Although strides have been made to understand the structure and function of nitrogenases, many questions remain regarding the underlying reasons for differential reduction capabilities between these two variants. This research aims to understand the biochemistry behind the unique capabilities of V-nitrogenase.

Table 1.1: Substrates and rates of catalysis for Mo- and V-nitrogenase. All activities are listed in nmol product/nmol catalytic protein/minute.

Substrate	Mo-nitrogenase rates for potential products	V-nitrogenase rates for potential products	Ref.
Nitrogen (N_2)	NH_3: 205 ± 5 H_2: 133 ± 8	NH_3: 111 ± 10 H_2: 192 ± 7	52
Protons (H^+)	H_2: 489 ± 34	H_2: 419 ± 8	52
Acetylene (C_2H_2)	C_2H_4: 483 ± 19	C_2H_4: 136 ± 3 C_2H_6: 4 ± 1	52
Carbon monoxide (CO)	C_2H_4: 0.00552 C_2H_6: 0.00276 C_3H_6: 0.000640 C_3H_8: 0.00129	CH_4: 0.124 C_2H_4: 7.74 C_2H_6: 0.244 C_3H_6: 0.0105 C_3H_8: 0.137 C_4H_8: 0.000512 C_4H_{10}: 0.000809	53

1.8 Research methods overview

The research described herein spans various projects that center around understanding the biochemistry of the differential reduction capabilities of the Mo- and V-nitrogenases. For this purpose, typical experimental methods include purification of proteins, extraction of catalytic cofactors, activity assays, and physical sample characterization through spectroscopic methods. Brief descriptions of relevant experimental methods are provided below. Additional information regarding research methods is provided at the end of each subsequent chapter.

1.8.1 Preparation of proteins and isolated cofactors

Initially, proteins are produced in the native bacterial host *A. vinelandii* or expressed heterologously in *Escherichia coli* (*E. coli)*. For production in *A. vinelandii,* strains expressing His-tagged NifDK, VnfDGK, and non-tagged NifH or VnfH are grown and purified using previously reported methods.[27,58,59] The *A. vinelandii* strain used to produce His-tagged NifDK (DJ1141) is rifampicin-tolerant to facilitate growth without contamination.[60] Although DJ1141 contains genes for expression of the other nitrogenase variants, expression of Mo-nitrogenase is activated by supplying a molybdenum salt (Na_2MoO_4) to the growth media. The His-tagged VnfDGK strain (YM68A) is also rifampicin-tolerant. This strain is also a knock-out of *nifHDK* (Δ*nifHDK*) to prevent production of Mo-nitrogenase. Expression of V-nitrogenase and biosynthesis of the V-cluster is facilitated by supplying a vanadium salt (Na_3VO_4) during growth. An additional strain (DJ1143, Δ*nifB*) is utilized to produce the cofactor-deficient apo-Mo-nitrogenase.[60]

A. vinelandii cells are grown in a 250 L aerobic fermenter in 180 L batches. Cells are supplied with Burke's minimal media supplemented with 2 mM ammonium acetate.[58] The growth media also includes an iron source ($Fe(III)Cl_3$) and either the vanadium or molybdenum salt. Cells are grown overnight, and optical density is monitored at 436 nm. Once the ammonium acetate source is depleted, expression of nitrogenase proteins is required for cell metabolism and growth, and cell division slows due to increased nitrogenase expression. Cells are harvested during this lag phase of growth around A_{436} = 0.9. One growth cycle of DJ1141 or YM68A yields about 500 g of cell paste mass after centrifugation. The cell paste is mixed with 50 mM Tris-HCl (pH 8.0) and frozen on dry ice until purified.

Protein purification is subsequently conducted under anaerobic conditions. Standard purification buffers contain 50 mM Tris-HCl (pH 8.0), 10% glycerol (by volume), and 50-500 mM NaCl. All purification buffers are degassed while stirring on a vacuum-argon dual manifold Schlenk line for one hour prior to use. After degassing buffers for one hour, 2 mM $Na_2S_2O_4$ reductant is added to scavenge any remaining O_2, and buffers are degassed for an additional 10 minutes. Buffers are kept in an argon atmosphere after degassing and during use.

Purification of His-tagged proteins takes about five hours. A protein purification of His-tagged Mo- or V-nitrogenase begins with thawing and lysis of the cells. Cells are lysed twice in an argon-filled 110 L capacity microfluidizer. The cell lysate is centrifuged to remove the cell debris from the supernatant. After centrifugation, the supernatant is loaded onto a Ni-Sepharose column. Non-specific binding is mitigated by washing the column with 40 mM imidazole and 500 mM NaCl. Proteins are eluted with 250 mM imidazole. Purified protein samples are frozen as pellets in liquid N_2 and stored in liquid N_2-filled dewars until further use. Yields from purification of Mo- or V-nitrogenase are roughly 1 mg protein/1 g of cell mass, and so one growth cycle in the 250 L fermenter yields about 500 mg of pure protein. Once frozen, proteins are stable over long periods.[58,59]

Untagged Fe proteins (NifH or VnfH) are purified by loading the Ni-Sepharose flow-through mixture onto a Q-Sepharose column, washing with 50 mM Tris-HCl (pH 8.0), and eluting with 500 mM NaCl and 50 mM Tris-HCl (pH 8.0). The eluted mixture is loaded onto Sephacryl S-200 SF size exclusion columns and run overnight in 50 mM Tris-HCl (pH 8.0) with 100 mM NaCl. The NifH or VnfH protein fractions are collected by monitoring

the elution profile at 405 nm. The Fe-protein fraction is then loaded onto a Q-Sepharose column and eluted by a linear NaCl gradient (100 mM to 500 mM). Purification of untagged reductase proteins can take two or more days depending upon whether or not multiple batches of Ni-Sepharose flow-through are utilized. Purified proteins are frozen as pellets in liquid N_2 and stored in liquid N_2-filled dewars.[58,59]

Some nitrogenase cofactors (L-, V-, and M-clusters) can be isolated from their respective protein scaffolds. In this method, purified Mo- or V-nitrogenase is prepared for cofactor extraction by removal of imidazole and glycerol. The catalytic cofactors are extracted from the protein scaffold by gently precipitating the protein with acid and extracting the cofactors in organic solvent (NMF) with 1,4-benzenedithiol as an extraction ligand. The resulting extraction mixture is concentrated under reduced pressure. This process takes about 12 hours and must be completed under strictly anaerobic conditions.[61,62] Extracted cofactors can be catalytically active under certain reaction conditions.[51,61–63]

1.8.2 Activity assays and product analysis

Once purified, catalytic nitrogenase proteins are combined with various substrates in the presence of a reductant and an ATP-regenerating system that allows reactions to occur without the native ferredoxin and flavodoxin partners. Activity assays are conducted under air-free conditions in sealed vials pressurized with Ar or a gaseous substrate. Samples can also be handled in Ar-filled glove boxes in which the concentration of O_2 is less than 4 parts per million (ppm). The reaction vials contain catalytic and reductase proteins, the ATP regenerating mixture, 20 mM DT, and substrate. Reaction vials are incubated with continuous shaking in a water bath at 30 °C. After completion, the

reactions are quenched with 100 μL of 30% trichloroacetic acid (TCA) and the headspace or liquid is analyzed for various products. These *in vitro* activity assays can be used to test the capabilities of nitrogenase variants under a wide array of experimental conditions. Activity assays can be used to experiment with different sets of catalytic and reductase protein components (from *A. vinelandii* or other organisms), molar ratios of catalytic and reductase components, substrates and substrate concentrations, reaction temperature, reaction time, reductant source and concentration, and other experimental factors.

Another method utilizes nitrogenase cofactor biosynthesis to mature incomplete cofactors *in vitro*. This maturation process requires a suite of purified nitrogenase proteins including NifEN, NifH, and apo-NifDK (Δ*nifB* NifDK). Sources of molybdenum (molybdate, $[MoO_4]^{2-}$) and homocitrate (as a racemic mixture of (*R*)- and (*S*)-homocitrate) are included to mature the L-cluster on NifEN into the complete M-cluster. The generated M-cluster is transferred to the apo-NifDK and is evaluated based upon the resulting catalytic activities. This method also requires an ATP source and a reductant. Maturation assays allow for additional experimentation and manipulation of the nitrogenase cofactor. For example, alternative metals or organic ligands can be provided to alter the resulting cofactor structure and reactivity.[64]

Extracted cofactors can be used to reconstitute apo-NifDK by mixing both components together. Once reconstituted with cofactor, apo-NifDK becomes holo-NifDK and can successfully reduce substrates.[61,63] This method is used to study the reactivity of extracted cofactors from nitrogenase variants in the context of a common protein scaffold (Δ*nifB* NifDK). Apart from demonstrating reactivity within the Δ*nifB* NifDK protein scaffold, the cofactors also demonstrate activity when treated with stronger lanthanide

reductants such as Eu^{II}-DTPA (DTPA=diethylenetriaminepentaacetate) or SmI_2. Under these reaction conditions, isolated cofactors were shown to convert C_1 substrates (CO, CO_2 and CN^-) into small hydrocarbon products[51,65–67] In summary, these three *in vitro* systems (whole protein, reconstituted proteins, and isolated cofactors) allow for a wide array of experimental techniques with which to probe the capabilities of different nitrogenase variants and mutants.

After reduction of various substrates, products are typically detected and quantified by gas chromatography (GC). Hydrocarbon products are typically measured by GC with flame ionization detection (GC-FID), which separates headspace gases on an alumina column and utilizes combustion to quantify hydrocarbons. Hydrogen gas and other reducing gases are measured by GC with reducing gas detection (GC-RGD), which detects reducing gases based on reduction of mercury oxide. An additional instrument, which combines a GC with a mass spectrometer (GC-MS), can be used to detect a wide array of products. This multi-use instrument can be equipped with different columns that utilize unique stationary phases to separate products of varying polarity or size. Additionally, GC-MS is utilized to confirm origins of detected products through the use of labeled substrates, additives, and solvents. When isotope-labeled materials are incorporated into the reaction products, the resulting mass shift can be observed and analyzed to confirm which materials are being used as substrates during catalysis. Ammonium is detected by a high performance liquid chromatography fluorescence method.[68,69]

1.8.3 Physical Characterization: Electron Paramagnetic Resonance (EPR) Spectroscopy

The cofactors within purified proteins can be analyzed by electron paramagnetic resonance (EPR) spectroscopy. Observation of well-resolved EPR signals from nitrogenase proteins typically requires measurements to be conducted at cryogenic temperatures. With this method, unpaired electrons are probed by irradiating a sample with microwave energy in the presence of an external magnetic field. By scanning the magnetic field with constant microwave energy, an electron spin flip transition can be

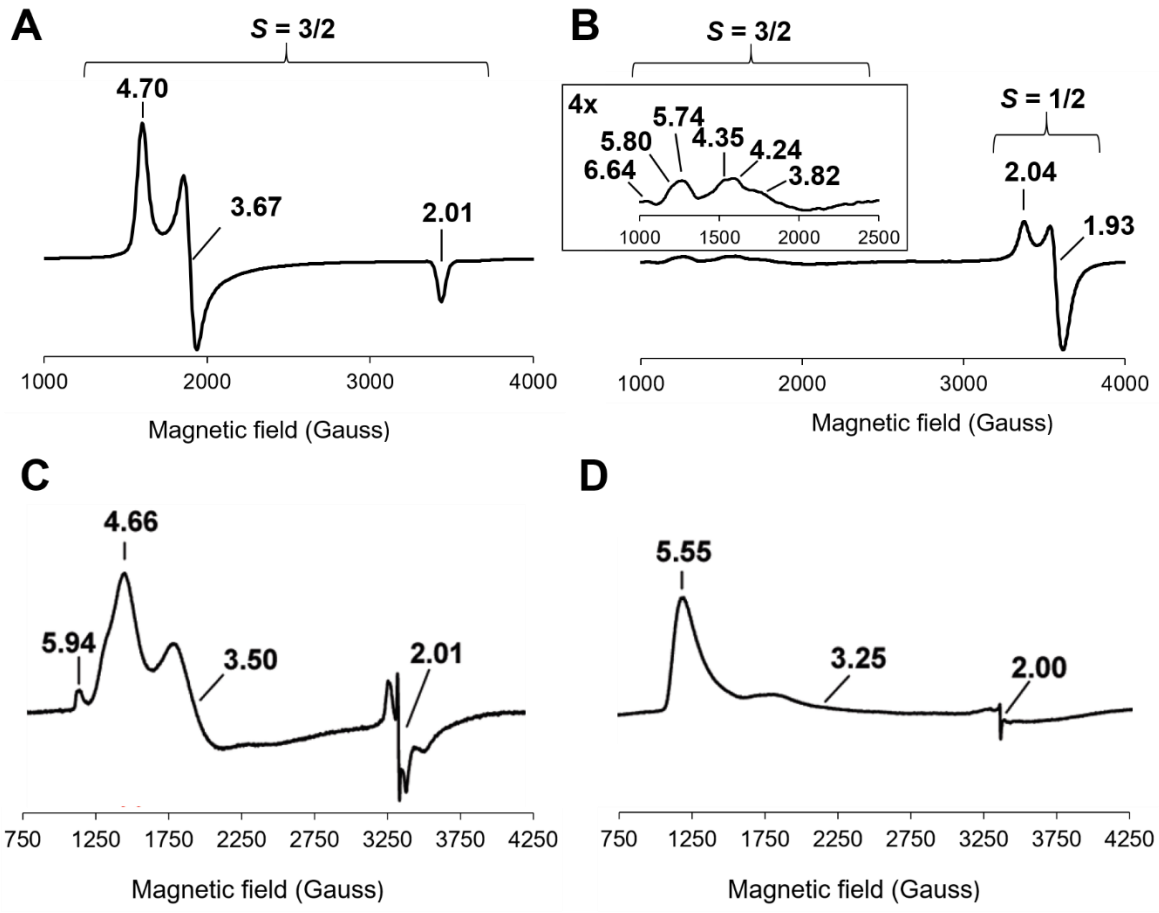

Figure 1.5: Perpendicular mode EPR of **A**) NifDK, **B**) VnfDGK, **C**) extracted M-cluster from NifDK in NMF, and **D**) extracted V-cluster from VnfDGK in NMF. Spectra A-C collected at 15K and 50mW; D collected at 6K and 50mW.[62]

observed. The resulting spin flips give spectra that indicate the overall spin state of the cofactors within purified proteins. Observed signals are characterized by *g*-values derived from the applied microwave wavelength and magnetic field. Typically, *g*-values are used to determine properties of unpaired electrons to provide a measure of the overall spin state. This information is utilized to verify that purified proteins contain the expected cofactors and that issues during biosynthesis or purification have not led to the formation of defective catalytic machinery. Additionally, EPR analysis can provide valuable information regarding the overall oxidation state of various nitrogenase cofactors by treating purified proteins with reductants or oxidants.

A perpendicular-mode spectrum of purified Mo-nitrogenase indicates that the M-cluster has an overall rhombic $S = 3/2$ signal with *g* values at $g = 4.70$, 3.67, and 2.01 under dithionite-reduced conditions (Figure 1.5A).[3] Extracted M-cluster retains characteristics of the $S = 3/2$ signal ($g = 4.66$, 3.5, and 2.01), and removal of the protein scaffold leads to broadened signal features, presumably due to an altered ligand environment (Figure 1.5C).[62,70]

The perpendicular-mode EPR spectrum of purified V-nitrogenase has been interpreted as overlapping signals originating from $S = 3/2$ and $S = 1/2$ (Figure 1.5B).[71,72] The intricate $S = 3/2$ signal has been assigned to the V-cluster, but the complete origin of the features within the $S = 3/2$ signal is unclear.[71,72] The dominant $S = 1/2$ signal ($g = 2.04$ and 1.93) has been assigned to signals associated with the P-cluster.[11,52] Interestingly, the extracted V-cluster retains a $S = 3/2$ signal with altered *g* values ($g = 5.55$, 3.25, and 2.00, Figure 1.5D).[62]

1.9 Research goals and aims

Mo- and V-nitrogenase differ from each other in their catalytic rates and reduction products from various substrates. Some of these reactions, such as the production of bioavailable NH_3 for fertilizer and the conversion of the pollutant CO into hydrocarbon fuel products, are of interest due to their potential applications for addressing global problems. V-nitrogenase demonstrates unique capabilities in terms of converting CO into fuel-like products, and a complete understanding of the biochemical properties that lead to this characteristic can aid in development of biological solutions for CO sequestration and recycling. The catalytic differences between Mo- and V-nitrogenase likely result from dissimilar protein compositions as well as the structures and properties of the active-site cofactors. A more thorough understanding of the structure-function relationships of these nitrogenases could provide insights into how to artificially control and improve the catalytic activity of nitrogenases.

In this context, the research described in this thesis attempts to clarify these differences in four separate aims:

1) Combining the protein scaffold of the V-nitrogenase with the cofactor of the Mo-nitrogenase (M-cluster) through *in vivo* growth experiments (Chapter 2). This nitrogenase hybrid was analyzed using whole protein assays and by extracting the M-cluster from the hybrid and using the cofactor to reconstitute apo-NifDK. Experiments utilizing CO as a substrate indicated that the protein scaffold of V-nitrogenase contributes significantly to its hydrocarbon-production capabilities.

2) Altering the organic ligand of V-nitrogenase though deletion of *nifV* to determine the resulting influences on enzymatic activity (Chapter 3). GC-MS analysis was used to identify the alternative ligand as citrate. Experiments utilizing the Δ*nifV* V-nitrogenase indicate that a shortened ligand backbone increases the production of NH_3 from N_2 reduction.

3) Extracting the catalytic cofactor from the V-nitrogenase *nifV* deletion mutant and using the extracted cofactor to reconstitute apo-NifDK (Chapter 4). The reconstituted protein mirrors the reactivity of the whole Δ*nifV* V-nitrogenase protein, indicating that the results observed with Δ*nifV* V-nitrogenase are a result of the altered organic ligand within the V-cluster.

4) Characterization of apo-NifDK reconstituted with extracted V- and M-clusters (Chapter 5). Reconstituted proteins were tested for their ability to convert CO into hydrocarbons in the presence of H_2O and D_2O. These studies indicate that the protein scaffold of V-nitrogenase contributes to its CO-reducing capabilities but that the isolated V-cluster maintains some features of the whole V-nitrogenase.

1.10 References

(1) *NASA Technical Reports Server (NTRS) - U.S. Standard Atmosphere, 1976*; 1976.

(2) Schlögl, R. *Angew. Chem. Int. Ed.* **2003**, *42* (18), 2004–2008.

(3) Burgess, B. K.; Lowe, D. J. *Chem. Rev.* **1996**, *96* (7), 2983–3012.

(4) Watt, G. D.; Burns, A. *Biochemistry* **1977**, *16* (2), 264–270.

(5) Seefeldt, L. C.; Hoffman, B. M.; Peters, J. W.; Raugei, S.; Beratan, D. N.; Antony, E.; Dean, D. R. *Acc. Chem. Res.* **2018**, *51* (9), 2179–2186.

(6) Howard, J. B.; Rees, D. C. *Chem. Rev.* **1996**, *96* (7), 2965–2982.

(7) Rivera Ortiz, J. M.; Burris, R. H. *J. Bacteriol.* **1975**, *123* (2), 537–545.

(8) Hardy, R. W. F.; Holsten, R. D.; Jackson, E. K. *Plant Physiol.* **1968**, *43*, 1185–1207.

(9) Hardy, R. W. F.; Burns, R. C.; Holsten, R. D. *Soil Biol. Biochem.* **1973**, *5* (1), 47–81.

(10) Lee, C. C.; Hu, Y.; Ribbe, M. W. *Science* **2010**, *329* (5992), 642.

(11) Eady, R. R. *Chem. Rev.* **1996**, *96* (7), 3013–3030.

(12) Joerger, R. D.; Bishop, P. E. *Crit. Rev. Microbiol.* **1988**, *16* (1), 1–14.

(13) Hu, Y.; Ribbe, M. W. *Annu. Rev. Biochem.* **2016**, *85* (1), 455–483.

(14) Schindelin, H.; Kisker, C.; Schlessman, J. L.; Howard, J. B.; Rees, D. C. *Nature* **1997**, *387* (6631), 370–376.

(15) Georgiadis, M. M.; Komiya, H.; Chakrabarti, P.; Woo, D.; Kornuc, J. J.; Rees, D. C. *Science* **1992**, *257* (5077), 1653–1659.

(16) Hu, Y.; Corbett, M. C.; Fay, A. W.; Webber, J. A.; Hodgson, K. O.; Hedman, B.; Ribbe, M. W. *Proc. Natl. Acad. Sci.* **2006**, *103* (46), 17125–17130.

(17) Jasniewski, A. J.; Sickerman, N. S.; Hu, Y.; Ribbe, M. W. *Inorganics* **2018**, *6* (1), 25.

(18) Kim, J.; Rees, D. C. *Science* **1992**, *257* (5077), 1677–1682.

(19) Spatzal, T.; Aksoyoglu, M.; Zhang, L.; Andrade, S. L.; Schleicher, E.; Weber, S.; Rees, D. C.; Einsle, O. *Science* **2011**, *334* (6058), 940–940.

(20) Sickerman, N. S.; Ribbe, M. W.; Hu, Y. *Acc. Chem. Res.* **2017**, *50* (11), 2834–2841.

(21) Hoover, T. R.; Imperial, J.; Ludden, P. W.; Shah, V. K. *Biochemistry* **1989**, *28* (7), 2768–2771.

(22) Madden, M. S.; Paustian, T. D.; Ludden, P. W.; Shah, V. K. *J. Bacteriol.* **1991**, *173* (17), 5403–5405.

(23) Masukawa, H.; Inoue, K.; Sakurai, H. *Appl. Environ. Microbiol.* **2007**, *73* (23), 7562–7570.

(24) Mayer, S. M.; Gormal, C. A.; Smith, B. E.; Lawson, D. M. *J. Biol. Chem.* **2002**, *277* (38), 35263–35266.

(25) Hu, Y.; Ribbe, M. W. *Coord. Chem. Rev.* **2011**, *255* (9–10), 1218–1224.

(26) Durrant, M. C.; Francis, A.; Lowe, D. J.; Newton, W. E.; Fisher, K. *Biochem. J.* **2006**, *397* (2), 261–270.

(27) Hu, Y.; Fay, A. W.; Dos Santos, P. C.; Naderi, F.; Ribbe, M. W. *J. Biol. Chem.* **2004**, *279* (52), 54963–54971.

(28) Hu, Y.; Corbett, M. C.; Fay, A. W.; Webber, J. A.; Hodgson, K. O.; Hedman, B.; Ribbe, M. W. *Proc. Natl. Acad. Sci.* **2006**, *103* (46), 17119–17124.

(29) Cabello, C. M.; Bair, W. B.; Lamore, S. D.; Ley, S.; Alexandra, S.; Azimian, S.; Wondrak, G. T. *J. Am. Chem. Soc.* **2010**, *46* (2), 220–231.

(30) Rettberg, L.; Tanifuji, K.; Jasniewski, A.; Ribbe, M. W.; Hu, Y. In *Methods in Enzymology*; Academic Press Inc., 2018; Vol. 606, pp 341–361.

(31) Rettberg, L. A.; Wilcoxen, J.; Lee, C. C.; Stiebritz, M. T.; Tanifuji, K.; Britt, R. D.; Hu, Y. *Nat. Commun.* **2018**, *9* (1), 2824.

(32) Wiig, J. A.; Hu, Y.; Lee, C. C.; Ribbe, M. W. *Science* **2012**, *337* (6102), 1672–1675.

(33) Wiig, J. A.; Lee, C. C.; Hu, Y.; Ribbe, M. W. *J. Am. Chem. Soc.* **2013**, *135* (13), 4982–4983.

(34) Martin, A. E.; Burgess, B. K.; Iismaa, S. E.; Smartt, C. T.; Jacobson, M. R.; Dean, D. R. *J. Bacteriol.* **1989**, *171* (6), 3162–3167.

(35) Chen, L.; Gavini, N.; Tsuruta, H.; Eliezer, D.; Burgess, B. K.; Doniach, S.; Hodgson, K. O. *J. Biol. Chem.* **1994**, *269* (5), 3290–3294.

(36) Jang, S. B.; Seefeldt, L. C.; Peters, J. W. *Biochemistry* **2000**, *39* (48), 14745–14752.

(37) Lanzilotta, W. N.; Ryle, M. J.; Seefeldt, L. C. *Biochemistry* **1995**, *34* (34), 10713–10723.

(38) Kim, J.; Rees, D. C. *Nature* **1992**, *360* (6404), 553–560.

(39) Bulen, W. A.; LeComte, J. R. *Proc. Natl. Acad. Sci.* **1966**, *56* (3), 979–986.

(40) Dance, I. *Dalt. Trans.* **2012**, *41* (25), 7647–7659.

(41) Spatzal, T.; Perez, K. A.; Einsle, O.; Howard, J. B.; Rees, D. C. *Science* **2014**,

345 (6204), 1620–1623.

(42) Spatzal, T.; Perez, K. A.; Howard, J. B.; Rees, D. C. *Elife* **2015**, *4* (e11620).

(43) Dance, I. *Dalt. Trans.* **2016**, *45* (36), 14285–14300.

(44) Hales, B. J.; Case, E. E.; Morningstar, J. E.; Dzeda, M. F.; Mauterer, L. A. *Biochemistry* **1986**, *25* (23), 7251–7255.

(45) Chisnell, J. R.; Premakumar, R.; Bishop, P. E. *J. Bacteriol.* **1988**, *170* (1), 27–33.

(46) Hales, B. J. *Adv. Inorg. Biochem.* **1990**, *8*, 165–198.

(47) Sippel, D.; Einsle, O. *Nat. Chem. Biol.* **2017**, *13* (9), 956–960.

(48) Hu, Y.; Lee, C. C.; Ribbe, M. W. *Dalt. Trans.* **2012**, *41* (4), 1118–1127.

(49) Benediktsson, B.; Thorhallsson, A. T.; Bjornsson, R. *Chem. Commun.* **2018**, *54* (53), 7310–7313.

(50) Sippel, D.; Rohde, M.; Netzer, J.; Trncik, C.; Gies, J.; Grunau, K.; Djurdjevic, I.; Decamps, L.; Andrade, S. L. A.; Einsle, O. *Science* **2018**, *359* (6383), 1484–1489.

(51) Lee, C. C.; Hu, Y.; Ribbe, M. W. *Angew. Chem. Int. Ed.* **2015**, *54* (4), 1219–1222.

(52) Lee, C. C.; Hu, Y.; Ribbe, M. W. *Proc. Natl. Acad. Sci.* **2009**, *106* (23), 9209–9214.

(53) Hu, Y.; Lee, C. C.; Ribbe, M. W. *Science* **2011**, *333* (6043), 753–755.

(54) Eady, R. R.; Richardson, T. H.; Miller, R. W.; Hawkins, M.; Lowe, D. J. *Biochem. J.* **1988**, *256* (1), 189–196.

(55) Bergström, J.; Eady, R. R.; Thorneley, R. N. *Biochem. J.* **1988**, *251* (1), 165–169.

(56) Hoffman, B. M.; Lukoyanov, D.; Yang, Z. Y.; Dean, D. R.; Seefeldt, L. C. *Chem. Rev.* **2014**, *114* (8), 4041–4062.

(57) Rebelein, J. G.; Lee, C. C.; Newcomb, M.; Hu, Y.; Ribbe, M. W. *MBio* **2018**, *9* (2).

(58) Burgess, B. K.; Jacobs, D. B.; Stiefel, E. I. *Biochim. Biophys. Acta* **1980**, *614* (1), 196–209.

(59) Ribbe, M. W. *Nitrogen fixation : methods and protocols*; Humana, 2011.

(60) Christiansen, J.; Goodwin, P. J.; Lanzilotta, W. N.; Seefeldt, L. C.; Dean, D. R. *Biochemistry* **1998**, *37* (36), 12611–12623.

(61) Shah, V. K.; Brill, W. J. *Proc. Natl. Acad. Sci.* **1977**, *74* (8), 3249–3253.

(62) Fay, A. W.; Blank, M. A.; Lee, C. C.; Hu, Y.; Hodgson, K. O.; Hedman, B.; Ribbe, M. W. *J. Am. Chem. Soc.* **2010**, *132* (36), 12612–12618.

(63) Pienkos, P. T.; Shah, V. K.; Brill, W. J. *Proc. Natl. Acad. Sci.* **1977**, *74* (12), 5468–5471.

(64) Yoshizawa, J. M.; Fay, A. W.; Lee, C. C.; Hu, Y.; Ribbe, M. W. *J. Biol. Inorg. Chem.* **2010**, *15* (3), 421–428.

(65) Lee, C. C.; Hu, Y.; Ribbe, M. W. *Angew. Chem. Int. Ed.* **2012**, *51* (8), 1947–1949.

(66) Sickerman, N. S.; Tanifuji, K.; Lee, C. C.; Ohki, Y.; Tatsumi, K.; Ribbe, M. W.; Hu, Y. *J. Am. Chem. Soc.* **2017**, *139* (2), 603–606.

(67) Tanifuji, K.; Sickerman, N.; Lee, C. C.; Nagasawa, T.; Miyazaki, K.; Ohki, Y.; Tatsumi, K.; Hu, Y.; Ribbe, M. W. *Angew. Chem. Int. Ed.* **2016**, *55* (50), 15633–15636.

(68) Corbin, J. L. *Appl. Environ. Microbiol.* **1984**, *47* (5), 1027–1030.

(69) Gavini, N.; Burgess, B. K. *J. Biol. Chem.* **1992**, *267* (29), 21179–21186.

(70) Spatzal, T.; Andrade, S. L. A.; Einsle, O. In *Characterization, Properties and Applications*; 2017; Vol. 1, pp 205–221.

(71) Morningstar, J. E.; Hales, B. J. *J. Am. Chem. Soc.* **1987**, *109* (22), 6854–6855.

(72) Sippel, D.; Schlesier, J.; Rohde, M.; Trncik, C.; Decamps, L.; Djurdjevic, I.; Spatzal, T.; Andrade, S. L. A.; Einsle, O. *J. Biol. Inorg. Chem.* **2017**, *22* (1), 161–168.

Chapter 2:

Characterization of an M-cluster-substituted nitrogenase VFe protein

2.1 Abstract

The Mo- and V-nitrogenases are two homologous members of the nitrogenase family that are distinguished mainly by the presence of different heterometals (Mo or V) at their respective cofactor sites (M- or V-cluster). However, the V-nitrogenase is ~600-fold more active than its Mo counterpart in reducing CO to hydrocarbons at ambient conditions. Here, we expressed an M-cluster-containing, hybrid V-nitrogenase in *Azotobacter vinelandii* and compared it to its native, V-cluster-containing counterpart in order to assess the impact of protein scaffold and cofactor species on the differential reactivities of Mo- and V-nitrogenases toward CO. Housed in the VFe protein component of V-nitrogenase, the M-cluster displayed electron paramagnetic resonance (EPR) features similar to those of the V-cluster and demonstrated an ~100-fold increase in hydrocarbon formation activity from CO reduction, suggesting a significant impact of protein environment on the overall CO-reducing activity of nitrogenase. On the other hand, the M-cluster was still ~6-fold less active than the V-cluster in the same protein scaffold, and it retained its inability to form detectable amounts of methane from CO reduction, illustrating a fine-tuning effect of the cofactor properties on this nitrogenase-catalyzed reaction. Together, these results provided important insights into the two major determinants for the enzymatic activity of CO reduction while establishing a useful framework for further elucidation of the essential catalytic elements for the CO reactivity of nitrogenase.

This is the first report on the *in vivo* generation and *in vitro* characterization of an M-cluster-containing V-nitrogenase hybrid. The “normalization” of the protein scaffold to that of the V-nitrogenase permits a direct comparison between the cofactor species of the

Mo- and V-nitrogenases (M- and V-clusters) in CO reduction, whereas the discrepancy between the protein scaffolds of the Mo- and V-nitrogenases (MoFe and VFe proteins) housing the same cofactor (M-cluster) allows for an effective assessment of the impact of the protein environment on the CO reactivity of nitrogenase. The results of this study provide a first look into the "weighted" contributions of protein environment and cofactor properties to the overall activity of CO reduction; more importantly, they establish a useful platform for further investigation of the structural elements attributing to the CO-reducing activity of nitrogenase.

2.2 Introduction

Nitrogenase is an important metalloenzyme that catalyzes certain remarkable chemical transformations under ambient conditions.[1] Catalysis by nitrogenase is enabled by ATP-dependent transfer of electrons from a reductase component to a catalytic component of the enzyme, followed by the subsequent reduction of substrates at the cofactor site of the catalytic component upon accumulation of sufficient electrons.[2,3] Using this two-component mechanism, the nitrogenase is capable of reducing nitrogen (N_2) to ammonia (NH_3), as well as carbon monoxide (CO) to hydrocarbons (e.g., propane [C_3H_8] and butane [C_4H_{10}]) at ambient conditions.[4,5] Interestingly, these two reactions parallel the industrial Haber-Bosch and Fischer-Tropsch processes, respectively, which are used for large-scale production of ammonia and carbon fuels. However, in contrast to the energy-demanding industrial processes, the enzymatic reactions occur under ambient temperatures and pressures.[6,7] The unique features of the nitrogenase-catalyzed reactions make them fascinating subjects of study from a perspective of chemical energy while suggesting the potential of using these systems as prototypes for future

development of biomimetic catalysts for energy- and cost-efficient production of useful chemical compounds.

The molybdenum (Mo)- and vanadium (V)-dependent nitrogenases are two homologous members of the nitrogenase family.[8] Mainly distinguished by the presence of a different heterometal (i.e., Mo or V) at the cofactor site, the two nitrogenases comprise a pair of homologous component proteins: a homodimeric reductase component (*nifH*- or *vnfH*-encoded Fe protein), which contains a subunit-bridging [Fe_4S_4] cluster and an MgATP-binding site within each subunit; and a multimeric catalytic component (*nifDK*-encoded MoFe protein or *vnfDGK*-encoded VFe protein), which contains an 8Fe P-cluster species (P- or P*-cluster) at each α/β-subunit interface and a 7Fe/1Mo or 7Fe/1V cofactor species (M- or V-cluster) within each α subunit.[9] Intriguingly, while biochemical, spectroscopic, and structural analyses reveal a striking resemblance between the Mo- and V-nitrogenases in terms of protein structure and cluster species, the two nitrogenase systems are clearly distinct in their catalytic behaviors.[9,10] Most notably, the Mo- and V-nitrogenases display significantly different reactivities toward the substrate CO, with the former showing a marginal activity of ~0.02 nmol of reduced carbon/nmol of protein/min, and the latter demonstrating a significantly increased activity at ~16 nmol of reduced carbon/nmol of protein/min—substantially higher than its Mo counterpart.[4,5] The observation of highly differential CO-reducing activities of two homologous nitrogenases has prompted us to define key features of these systems that contribute to this discrepancy in activity; in particular, the question of whether the protein environment or the cofactor species determines the reactivity of nitrogenase toward CO needs to be addressed, as knowledge in this regard represents the first step toward understanding

the CO-reducing activity of nitrogenase for the potential applications of this reactivity in the future.

2.3 Results

To tackle the question in hand, the M- and V-clusters must be placed in the same protein environment for direct comparison. Using a genetically altered *Azotobacter vinelandii* strain, a pair of VFe proteins containing either the V- or M-cluster can be generated *in vivo* for this line of investigation. This *A. vinelandii* strain expresses a His-tagged form of VFe protein in a genetic background that contains deletions of (i) the *nifDK* genes, which encode the MoFe protein, and (ii) the *mod* genes, which encode the Mo uptake system (locus tag Avin_50650-Avin_50730 of the *A. vinelandii* DJ strain).[11–14] Using this *A. vinelandii* strain, a V-cluster-containing native form of the VFe protein (designated VnfDGK^{V}) was produced *in vivo* when V was supplemented in the growth medium (Fig. 2.1A), where deletion of the Mo transporter prevented incorporation of trace Mo into the cofactor, whereas an M-cluster-containing hybrid form of the VFe protein (designated VnfDGK^{M}) was produced *in vivo* when Mo was added in excess to the growth medium (Fig. 2.1A), where the uptake of Mo was accomplished by other transporter systems, such as those involving siderophores.[12–16] Like the native VnfDGK^{V} protein, the VnfDGK^{M} hybrid consists of α, β, and δ subunits, although the δ subunit is present in a reduced quantity in VnfDGK^{M} than in VnfDGK^{V} (Fig. 2.1A). Metal analysis reveals a metal content of 0.9 nmol Mo and less than 0.07 nmol V per nmol protein (Fig. 2.1B), suggesting that VnfDGK^{M} houses an Mo-containing cofactor in place of a V-containing species. Not too surprisingly, the heterologous incorporation of

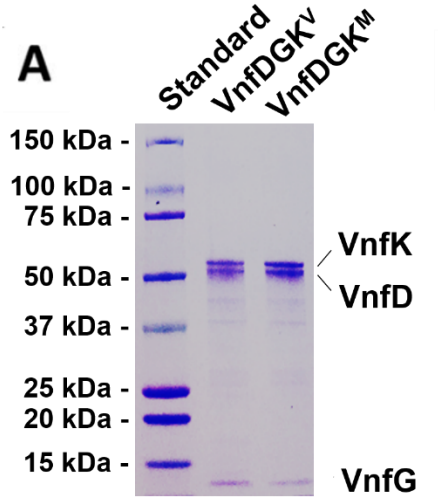

B

	Metals analysis (nmol metal/nmol protein)		
Protein	**Fe**	**Mo**	**V**
$NifDK^M$	29.3 ± 0.7	1.7 ± 0.1	<0.05
$VnfDGK^V$	27.8 ± 2.9	<0.01	1.5 ± 0.3
$VnfDGK^M$	23.5 ± 2.7	0.9 ± 0.1	<0.07

Figure 2.1: Subunit and metal compositions of $VnfDGK^V$ and $VnfDGK^M$. (**A**) SDS-PAGE analysis of $VnfDGK^V$ and $VnfDGK^M$. The molecular masses (in kilodaltons) of the protein standards are shown to the left of the gel. (**B**) Metal contents of $NifDK^M$, $VnfDGK^V$, and $VnfDGK^M$ as determined by ICP-OES.

the Mo-containing cofactor into the VnfDGK scaffold is less efficient than the homologous incorporation of the V-containing cofactor, as the Mo content of $VnfDGK^M$ supports the assignment of one M-cluster per protein, which is lower than the assignment of ~1.5 V-clusters per protein in the case of $VnfDGK^V$. The identity of the cofactor species in VnfDGKM is confirmed by extracting the cofactor from $VnfDGK^M$ into an organic solvent, *N*-methylformamide (NMF), and subsequently inserting it into the cofactor-deficient apo-NifDK (designated $NifDK^{apo}$). As shown in Fig 2.2A, the apo-NifDK protein reconstituted with the cofactor extracted from $VnfDGK^M$ (designated M^{VnfDGK}) exhibits EPR features (g = 4.31, 3.67, 2.01, and 1.91) identical to those of the $NifDK^{apo}$ protein reconstituted with the cofactor extracted from the wild-type NifDK (designated M^{NifDK}). Moreover, when combined with the reductase component (designated NifH), the M^{VnfDGK}- and M^{NifDK}-reconstituted $NifDK^{apo}$ proteins demonstrate nearly indistinguishable substrate-reducing activities when N_2, proton (H^+) or acetylene (C_2H_2) is supplied as the

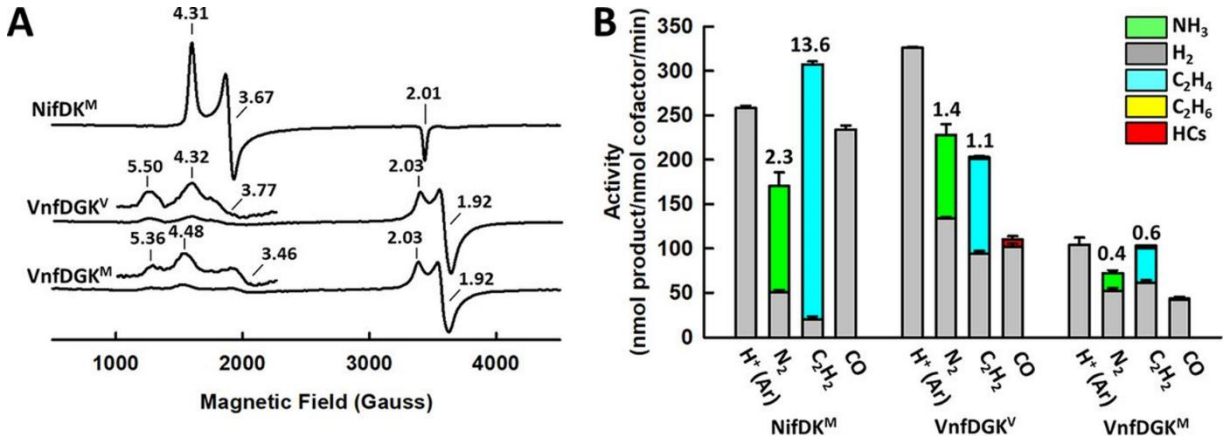

Figure 2.2: Spectroscopic and catalytic properties of NifDK^M, VnfDGK^V, and VnfDGK^M. EPR spectra (**A**) and activity profiles (**B**) of NifDK^M, VnfDGK^V, and VnfDGK^M. Note the presence of the same S = 1/2 signal in the spectra of VnfDGK^V and VnfDGK^M (see panel A), which was assigned to the P*-cluster (i.e., a pair of [Fe_4S_4]-like clusters) in the case of VnfDGK^V.[11] The g values are indicated in panel A, and the products are color coded in panel B. The substrates are indicated at the bottom of the bar chart.

substrate (Fig 2.2B). Together, these observations establish VnfDGK^M as an M-cluster-containing counterpart of VnfDGK^V.

Interestingly, the M-cluster in VnfDGK^M displays EPR features (g = 5.36, 4.48, and 3.46) similar to those of the native V-cluster in VnfDGK^V (g = 5.50, 4.32, and 3.77), both of which are clearly distinct from the EPR features of the native M-cluster in NifDK^M (g = 4.31 and 3.67) (Fig. 2.3A). This observation is interesting, as it highlights a strong impact of protein environment on the properties of the cofactor. Consistent with the observed similarity between their EPR features, VnfDGK^M seems to follow its native VnfDGK^V counterpart in terms of the overall product distribution patterns, demonstrating decreased NH_3/H_2 and C_2H_4/H_2 ratios relative to those generated by NifDK^M, the ability to generate C_2H_6 from C_2H_2 reduction that is absent from NifDK^M, and higher activity than

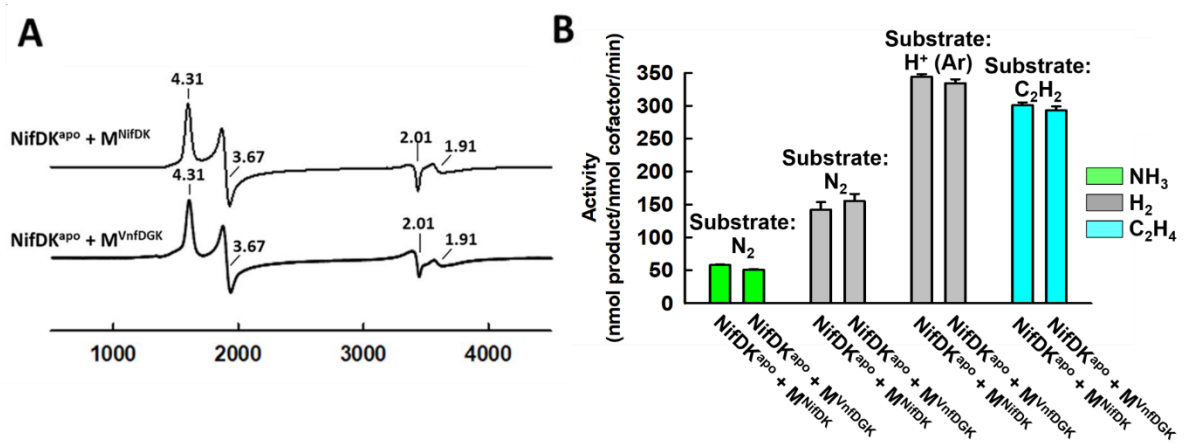

Figure 2.3: Spectroscopic and catalytic properties of the M-cluster extracted from VnfDGK^{M}. EPR spectra (**A**) and activity profiles (**B**) of the cofactor-deficient NifDK^{apo} protein reconstituted with the M-cluster extracted from NifDK (NifDK^{apo} + M^{NifDK}) or VnfDGK^{M} (NifDK^{apo} + M^{VnfDGK}). The *g* values are indicated in panel A. Activities are expressed as nanomoles of product per nanomole of cofactor per min in panel B.

NifDK^{M} in producing hydrocarbons from CO reduction (Fig. 2.3B).[4,5,8,11] The similarity between the CO reactivities of VnfDGK^{M} and VnfDGK^{V} is particularly striking. Both VnfDGK^{M} and VnfDGK^{V} reduce CO to hydrocarbons of up to C_4 in length, whereas in comparison, NifDK^{M} has a narrower product profile comprising up to C_3 hydrocarbons (Fig. 2.4A). Moreover, the product distribution profiles of VnfDGK^{M} and VnfDGKV are remarkably similar, with C_2H_4/C_2H_6 comprising 96.3%/2.5% and 94.6%/3.1%, respectively, of the total amounts of hydrocarbons generated by these proteins, displaying a clear tendency toward formation of the unsaturated C_2 product (C_2H_4); in contrast, NifDK^{M} generates C_2H_4/C_2H_6 at 56.9%/28.4% of the total amounts of hydrocarbons, showing a preference for formation of the saturated C_2 product (C_2H_6) (Fig. 2.4A). The protein environment, therefore, appears to “normalize” the product profiles of the M- and V-clusters in CO reduction once they are inserted into the same protein scaffold, VnfDGK. Further, the fact that VnfDGK^{M} is considerably more active than NifDK^{M} (by ~100-fold) in

CO reduction illustrates the higher efficiency of the VnfDGK scaffold in catalyzing this reaction (Fig. 2.4B).

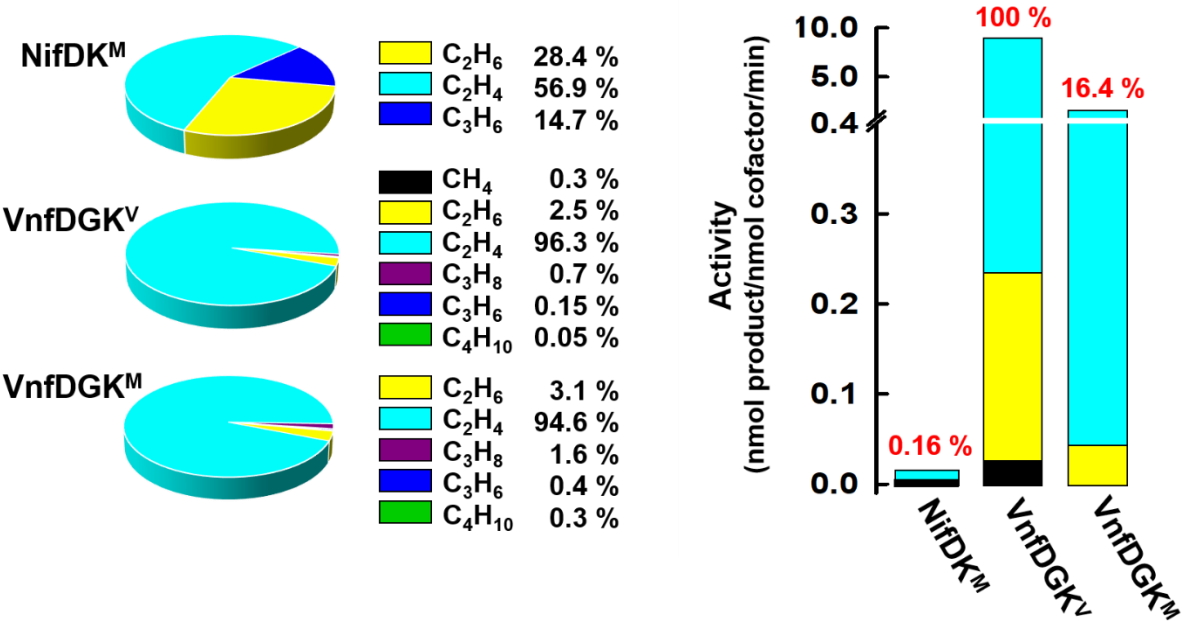

Figure 2.4: CO-reducing activities and product profiles of NifDK^M, VnfDGK^V, and VnfDGK^M. Distributions of hydrocarbon products (**A**) and total activities of hydrocarbon product formation (**B**) by NifDK^M, VnfDGK^V, and VnfDGK^M when CO is supplied as a substrate. Activities are expressed as nanomoles of product per nanomole of cofactor per minute. The percentage activities of proteins are shown in red in panel B, with the total activity of VnfDGK^V set at 100% and those of NifDK^M and VnfDGK^M calculated accordingly.

There is, however, a clear contribution of the cofactor properties to the CO-reducing activity, as VnfDGK^V is ~6-fold more active than VnfDGK^M in hydrocarbon formation, which demonstrates that the V-cluster is better tuned toward CO reduction than the M-cluster (Fig. 2.4B). Moreover, despite the "normalization" of the protein environment, the ability of VnfDGK^V to form detectable amounts of CH_4 is not observed in the case of VnfDGK^M under the same experimental conditions (Fig. 2.4A). Given the absence of CH_4 from the product profile of NifDK^M (Fig. 2.4A), this trait seems to be carried over to VnfDGK^M by the M-cluster, further highlighting the characteristics of the

unique properties of the M-cluster in the reaction of CO reduction. Taken together, these results suggest a combined effect of protein environment and cofactor properties on the reactivity of nitrogenase toward CO: the protein scaffold has a significant impact on the overall activity of CO reduction (Fig. 2.4B, VnfDGK^{M} versus NifDK^{M}), whereas the cofactor species fine-tunes the product profile of CO reduction while exerting a moderate impact on the overall activity (Fig. 2.4B, VnfDGK^{V} versus VnfDGK^{M}). It is interesting to note that a "weighted" contribution of protein environment and cofactor properties to the CO-reducing activity can be derived from these comparisons, with (i) the ~100-fold difference that arises from the difference in protein scaffold and (ii) the ~6-fold difference that arises from the difference in cofactor species contributing collectively to an ~600-fold difference between the CO-reducing activities of Mo- and V-nitrogenases.

2.4 Discussion

The impact of protein environment on the CO reactivity of nitrogenase is intimately associated with the immediate surroundings of the cofactor that could play a significant role in the interactions between the cofactor and the substrate CO. The cofactor "pocket" in the recently reported crystal structure of VnfDGK is slightly more polar than its counterpart in NifDK, which may influence the electrochemical properties of the cofactor.[17] Moreover, the cofactor captured in the crystal structure of VnfDGK has a "belt" sulfur substituted by a carbonate moiety.[17] A comparison between the cofactor-binding sites in the crystal structures of VnfDGK and NifDK reveals comparable hydrogen bonding networks around the homocitrate moieties of the two cofactors but markedly different hydrogen bonding at the position where carbonate is bound to the V-cluster, which could contribute to the differences in the catalytic activities of the two proteins.[17] Other than the

cofactor environment, the P-cluster species, which mediates electron transfer to the cofactor, could also impact the CO reactivity of nitrogenase. While the P-cluster in the crystal structure of VnfDGK is determined to have the same [Fe_8S_7] structure as its counterpart in NifDK, there are additional electron densities at the P-cluster site that suggest the possible existence of an additional P-cluster conformation(s) that is not populated or captured in the specific redox state of the VnfDGK crystal.[17] This observation is in line with the X-ray absorption spectroscopy (XAS)/extended X-ray absorption fine structure (EXAFS)-derived structure of the P-cluster of a cofactor-deficient VnfDGK, which suggests that this cluster assumes the conformation of a [Fe_4S_4]-like cluster pair in the solution state. It is likely, therefore, that the P-cluster of VnfDGK is capable of undergoing different conformational changes than those of its counterpart in NifDK upon redox changes. In this context, it is interesting to note that the P-cluster of the reduced, resting-state VnfDGK exhibits analogous $S = 1/2$ and $S = 5/2$ electron paramagnetic resonance (EPR) signals to the one-electron-oxidized, P^{1+} state of the P-cluster of NifDK, which has been implicated in substrate turnover.[8,18] Such a difference in redox states, likely associated with the conformational differences between the two P-cluster species, could very well impact the ability of the respective proteins to transfer electrons to their cofactor sites and, consequently, the catalytic activities of these proteins.

The impact of cofactor properties on the CO reactivity of nitrogenase, on the other hand, could stem from the presence of different heterometals in the M- and V-clusters. Interestingly, differential abilities of synthetic V- and Mo-containing compounds to reductively couple two CO moieties into functionalized acetylene ligands have been observed previously, which suggests a higher capacity of V (a first-row transition metal)

than Mo (a second-row transition metal) in this type of reactions.[19] While this observation may be used to account for the differential reactivities of V- and M-clusters toward CO, it remains unclear whether the heterometal directly participates in substrate reduction or exerts an indirect effect on the electronic/catalytic properties of the cofactor. Apart from the differential heterometal compositions of the V- and M-clusters, the presence of a carbonate moiety at the belt region of the V-cluster—a feature that is absent from any M-cluster structure reported so far—may also impact the nitrogenase reactivity.[17] The observed substitution of a belt sulfide of the V-cluster by carbonate is interesting, as carbonate is a potential carbon substrate of this cofactor. However, the sulfide displaced by carbonate in the structure of the V-cluster is different than the sulfide equivalent displaced by CO in the structure of the CO-bound M-cluster.[20] Moreover, a catalysis-dependent migration of belt sulfide has been suggested recently for the M-cluster, which could very well enable displacement of carbonate by a sulfide during substrate reduction in the case of the V-cluster.[21] This proposal is also consistent with our XAS/EXAFS-derived structure of the isolated V-cluster, where a sulfide is modeled in place of carbonate in the belt region of this cofactor.[22] The unlikely scenario that carbonate, a very weak ligand, has survived the cluster extraction procedure, along with the observation that the isolated V-cluster can be used to reconstitute cofactor-deficient proteins, suggests that a carbonate-free conformation of the V-cluster is likely the competent form in substrate reduction.[22] Clearly, the origin and catalytic relevance of the carbonate moiety needs to be clarified before mechanistic interpretations can be made based on this finding.

The *in vitro* formation of an M-cluster containing the VnfDGK hybrid and analysis

of its N_2-reducing activity was reported earlier.[23] However, the *in vivo* generation of this hybrid, which permits a direct comparison of the activities of hydrocarbon formation by the M- and V-cluster-containing VnfDGK proteins generated under cell growth conditions, has not been accomplished prior to the current study. Other than facilitating a direct assessment of the contributions of protein scaffold and cofactor species to the CO-reducing activity of nitrogenase, our *in vivo* generation of a heterologous form of VnfDGK that contains an M-cluster at its cofactor-binding site also sheds light on the regulation of nitrogenase expression and the biosynthesis of the "alternative" nitrogenase. It is interesting to note that, despite the deletion of the *mod*-encoded Mo uptake system in *A. vinelandii*, the cells still manage to acquire sufficient Mo from a growth medium supplemented with excess Mo for the synthesis of M-clusters.[11–14] In contrast to earlier suggestions, the expression of *vnf* genes in a *nifDK* deletion background is not suppressed by the amount of Mo taken up by this mechanism.[24] Moreover, unlike NifEN that is specific for M-cluster synthesis, VnfEN is apparently capable of synthesizing both M- and V-clusters for VnfDGK, further facilitating the formation of $VnfDGK^M$ via this approach.[25,26] Finally, there is an obvious reduction in the amount of the *vnfG*-encoded δ subunit in the $VnfDGK^M$ protein (Fig. 2.1A). This observation coincides with results derived from the characterization of a cofactor-deficient form of VnfDGK, which reveals the absence of the δ subunit and an incomplete, $\alpha\beta_2$-trimeric composition of this cofactor-less protein.[27] The positive correlation between the decreased amount of δ subunit and the absence of V-cluster suggests a possible role of the δ subunit in specifically delivering the V-cluster to the cofactor-binding site and maintaining the stability at the α/β subunit interface once its delivery job is finished.

While many aspects related to the expression and assembly of the alternative nitrogenase await investigation, the outcome of this work provides a useful framework for further investigation of the two major determinants—the protein environment and the cofactor species—in order to narrow down the key elements attributing to the CO reactivity of nitrogenase. Moreover, the strategy used in this work for the successful generation of VnfDGK^{M} *in vivo* could potentially be employed for generation of other heterologous forms of nitrogenase, which may facilitate further exploration of this unique reactivity of nitrogenase for potential applications in the future.

2.5 Materials and Methods

2.5.1 Strain construction and cell growth: *Azotobacter vinelandii* strains YM68A and YM13A (expressing His-tagged VnfDGK and NifDK, respectively) were constructed as described earlier.[11,28] Both strains were grown in 180-liter batches in a 200-liter New Brunswick fermenter (New Brunswick Scientific) in Burke's minimal medium supplemented with 2 mM ammonium acetate.[11,28] The molybdate in Burke's medium was replaced by an equal amount of vanadate for the expression of the native $VnfDGK^{V}$ protein in strain YM68A. In preparation for the expression of the $VnfDGK^{M}$ hybrid in strain YM68A, the fermenter was scrubbed with acid and water, followed by growth of two consecutive 180-liter batches of YM68A in Burke's medium that contained no Mo or V, which permitted removal of trace amounts of V in the vessel. Subsequently, strain YM68A was grown in Burke's medium supplemented with 2.5-fold molybdate, and cell growth was monitored by measuring the cell density at 436 nm using a Spectronic 20 Genesys spectrophotometer. Cells were harvested in the late exponential phase by a flow through centrifugal harvester (Cepa), and the cell paste was washed with a buffer containing 50 mM Tris-HCl (pH 8.0). Published methods were then used for the purification of His-tagged NifDK and VnfDGK and nontagged NifH and VnfH.[11,28]

2.5.2 Protein characterization and activity assays: VnfDGK proteins were subjected to sodium dodecyl sulfate-polyacrylamide gel electrophoresis (SDS-PAGE) analysis on a 4 to 20% precast Tris-glycine gel (Bio-Rad). The metal contents of the proteins were determined by inductively coupled plasma-optical emission spectroscopy (ICP-OES) based on previously established protocols.[29] All nitrogenase activity assays were carried out as described earlier.[30,31] The hydrocarbon products were analyzed as described

elsewhere.[4,5,29] Ammonium was determined by a high-performance liquid chromatography fluorescence method, and hydrogen was analyzed as described previously.[32,33]

2.5.3 Cofactor extraction and reconstitution of NifDK^{apo}: The NifDK- and VnfDGK^{M}-bound M-clusters were extracted into *N*-methylformamide (NMF) using a previously established method.[22] The extracted cofactor was then incubated with the M-cluster-deficient, apo-NifDK protein (NifDK^{apo}) for 20 min prior to removal of excess metal cluster by passing the reconstituted protein through a G25 column.

2.5.4 EPR spectroscopy: EPR samples were prepared in a Vacuum Atmospheres dry box at an oxygen level of <4 ppm. All samples contained 25 mM Tris-HCl (pH 8.0), 10% glycerol, and 2 mM sodium dithionite ($Na_2S_2O_4$). The EPR spectra were taken in perpendicular mode using a Bruker ESP 300 Ez spectrophotometer (Bruker) interfaced with an Oxford Instruments ESR-9002 liquid helium continuous flow cryostat. All spectra were recorded at 10 K, using a microwave power of 20 mW, a gain of 5×10^4, a modulation frequency of 100 kHz, and a modulation amplitude of 5 G. A microwave frequency of 9.62 GHz was used to collect five scans for each sample.

2.6 References

(1) Burgess, B. K.; Lowe, D. J. *Chem. Rev.* **1996**, *96* (7), 2983–3012.

(2) Rees, D. C.; Tezcan, F. A.; Haynes, C. A.; Walton, M. Y.; Andrade, S.; Einsle, O.; Howard, J. B. *Philos. Trans. Royal Soc. A* **2005**, *363* (1829), 971–984.

(3) Hoffman, B. M.; Lukoyanov, D.; Yang, Z. Y.; Dean, D. R.; Seefeldt, L. C. *Chem. Rev.* **2014**, *114* (8), 4041–4062.

(4) Lee, C. C.; Hu, Y.; Ribbe, M. W. *Science* **2010**, *329* (5992), 642.

(5) Hu, Y.; Lee, C. C.; Ribbe, M. W. *Science* **2011**, *333* (6043), 753–755.

(6) Rofer-DePoorter, C. K. *Chem. Rev.* **1981**, *81* (5), 447–474.

(7) Lee, C. C.; Hu, Y.; Ribbe, M. W. *Angew. Chem. Int. Ed.* **2011**, *50* (24), 5545–5547.

(8) Eady, R. R. *Chem. Rev.* **1996**, *96* (7), 3013–3030.

(9) Hu, Y.; Ribbe, M. W. *J. Biol. Inorg. Chem.* **2015**, *20* (2), 435–445.

(10) Hu, Y.; Ribbe, M. W. *Annu. Rev. Biochem.* **2016**, *85* (1), 455–483.

(11) Lee, C. C.; Hu, Y.; Ribbe, M. W. *Proc. Natl. Acad. Sci.* **2009**, *106* (23), 9209–9214.

(12) Bishop, P. E.; Jarlenski, D. M.; Hetherington, D. R. *Proc. Natl. Acad. Sci.* **1980**, *77* (12), 7342–7346.

(13) Bishop, P. E.; Jarlenski, D. M.; Hetherington, D. R. *J. Bacteriol.* **1982**, *150* (3), 1244–1251.

(14) Noar, J. D.; Bruno-Barcena, J. M. *Genome Announc.* **2013**, *1* (3).

(15) Kraepiel, A. M. L.; Bellenger, J. P.; Wichard, T.; Morel, F. M. M. *BioMetals* **2009**, *22* (4), 573–581.

(16) Thomas, W.; Bellenger, J. P.; Morel, F. M. M.; Kraepiel, A. M. L. *Environ. Sci. Technol.* **2009**, *43* (19), 7218–7224.

(17) Sippel, D.; Einsle, O. *Nat. Chem. Biol.* **2017**, *13* (9), 956–960.

(18) Rupnik, K.; Hu, Y.; Lee, C. C.; Wiig, J. A.; Ribbe, M. W.; Hales, B. J. *J. Am. Chem. Soc.* **2012**, *134* (33), 13749–13754.

(19) Carnahan, E. M.; Protasiewicz, J. D.; Lippard, S. J. *Acc. Chem. Res.* **1993**, *26* (3), 90–97.

(20) Spatzal, T.; Perez, K. A.; Einsle, O.; Howard, J. B.; Rees, D. C. *Science* **2014**, *345* (6204), 1620–1623.

(21) Spatzal, T.; Perez, K. A.; Howard, J. B.; Rees, D. C. *Elife* **2015**, *4* (e11620).

(22) Fay, A. W.; Blank, M. A.; Lee, C. C.; Hu, Y.; Hodgson, K. O.; Hedman, B.; Ribbe, M. W. *J. Am. Chem. Soc.* **2010**, *132* (36), 12612–12618.

(23) Moore, V. G.; Tittsworth, R. C.; Hales, B. J. *J. Am. Chem. Soc.* **1994**, *116* (26), 12101–12102.

(24) Burns, R. C.; Fuchsman, W. H.; Hardy, R. W. F. *Biochem. Biophys. Res. Commun.* **1971**, *42* (3), 353–358.

(25) Hu, Y.; Corbett, M. C.; Fay, A. W.; Webber, J. A.; Hodgson, K. O.; Hedman, B.; Ribbe, M. W. *Proc. Natl. Acad. Sci.* **2006**, *103* (46), 17119–17124.

(26) Yoshizawa, J. M.; Fay, A. W.; Lee, C. C.; Hu, Y.; Ribbe, M. W. *J. Biol. Inorg. Chem.* **2010**, *15* (3), 421–428.

(27) Blanchard, C. Z.; Hales, B. J. *Biochemistry* **1996**, *35* (2), 472–478.

(28) Hu, Y.; Fay, A. W.; Schmid, B.; Makar, B.; Ribbe, M. W. *J. Biol. Chem.* **2006**, *281* (41), 30534–30541.

(29) Sickerman, N. S.; Tanifuji, K.; Lee, C. C.; Ohki, Y.; Tatsumi, K.; Ribbe, M. W.; Hu, Y. *J. Am. Chem. Soc.* **2017**, *139* (2), 603–606.

(30) Hu, Y.; Fay, A. W.; Dos Santos, P. C.; Naderi, F.; Ribbe, M. W. *J. Biol. Chem.* **2004**, *279* (52), 54963–54971.

(31) Burgess, B. K.; Jacobs, D. B.; Stiefel, E. I. *Biochim. Biophys. Acta* **1980**, *614* (1), 196–209.

(32) Corbin, J. L. *Appl. Environ. Microbiol.* **1984**, *47* (5), 1027–1030.

(33) Gavini, N.; Burgess, B. K. *J. Biol. Chem.* **1992**, *267* (29), 21179–21186.

Chapter 3:

Characterization of a V-nitrogenase variant from *Azotobacter vinelandii* that contains a citrate-substituted cofactor

3.1 Abstract

Nitrogenase catalyzes the ambient reduction of N_2 and CO at its cofactor site. Here, we present biochemical and spectroscopic characterization of an *Azotobacter vinelandii* V-nitrogenase variant expressing a citrate-substituted cofactor. Designated VnfDGK^{Cit}, the catalytic component of this V-nitrogenase variant has an $\alpha\beta_2(\delta)$ subunit composition and carries an 8Fe P*-cluster and a citrate-substituted V-cluster analog in the αβ-dimer, as well as a 4Fe cluster in the 'orphaned' β-subunit. Interestingly, when substrate reduction activities are normalized based on the amount of catalytic cofactor, VnfDGK^{Cit} shows a shift of N_2-reduction from H_2-evolution toward NH_3-formation and an opposite shift of CO-reduction from hydrocarbon-formation toward H_2-evolution. These observations point to a role of the organic ligand in proton delivery during catalysis and imply the utilization of different reaction sites/mechanisms by nitrogenase for different substrate reductions. Moreover, the increased NH_3/H_2 ratio upon citrate substitution suggests the possibility to modify the organic ligand for improved ammonia synthesis in the future.

3.2 Introduction

Nitrogenase catalyzes the ambient transformation of N_2 to NH_3 as a key step in the global nitrogen cycle.[1] In addition, this enzyme is capable of ambient conversion of CO to hydrocarbons such as C_3H_8 and C_4H_{10}.[2,3] The ability of nitrogenase to catalyze Haber-Bosch- and Fischer-Tropsch-type reactions under ambient conditions makes this enzyme an important subject of study for understanding small molecule activation and developing biomimetic catalysts for energy-efficient production of useful chemical commodities.[4,5] Distinguished mainly by the heterometal at the active cofactor site, the

molybdenum (Mo)- and vanadium (V)-dependent nitrogenases are two homologous members of the nitrogenase enzyme family, both of which utilize a two-component mechanism for catalysis, transferring electrons concomitant with ATP hydrolysis from a reductase component to the cofactor site of a catalytic component to enable substrate reduction.[6–8] The homology between the two nitrogenases is reflected by the sequence and structural homology between their component proteins.[9–11] Specifically, the reductase components of the Mo- and V-nitrogenases (*i.e.*, the *nifH*- and *vnfH*-encoded Fe proteins) share 95% sequence homology and are structurally homologous homodimers containing a [Fe_4S_4] cluster between the subunits and an MgATP-binding site within each subunit. Similarly, the multimeric catalytic components of the Mo- and V-nitrogenases (*i.e.*, the *nifDK*-encoded MoFe protein and *vnfDGK*-encoded VFe protein) share 53% and 47% sequence homology between their respective α- and β-subunits and an overall homology in their tertiary structures; moreover, they both house a structurally homologous pair of cluster species, namely, an 8Fe P-cluster species (P- or P*-cluster) at the α/β-subunit interface and a 7Fe/1Mo or 7Fe/1V cofactor species (M- or V-cluster) within the α-subunit.

Interestingly, despite the significant degree of sequence and structural homology, the two nitrogenases are distinct in their catalytic capabilities. Most notably, the V-nitrogenase is less active than its Mo counterpart in N_2 reduction, and it generates NH_3 and H_2 as products of N_2 reduction at a substantially decreased ratio (NH_3/H_2=0.9) than its Mo counterpart (NH_3/H_2=2.3).[12] However, when CO is supplied as a substrate, the V-nitrogenase shows an activity of ~16 nanomole of reduced C/nanomole of catalytic protein/minute of reaction time (nmol C/nmol/min), whereas the Mo-nitrogenase only

shows a marginal activity of ~0.02 nmol of reduced C/nmol/min.[2,3] The observation of differential reactivities of the Mo- and V-nitrogenases toward the same substrate has prompted us to look into the differential properties of the two homologous cofactors in these proteins. Recently, direct comparisons of the M- and V-clusters were enabled by 'normalizing' the protein scaffold and comparing the catalytic activities either between the wildtype and M-cluster-substituted VFe proteins (generated *in vivo*) or between the wildtype and V-cluster-substituted MoFe proteins (generated *in vitro*).[13,14] In both cases, the overall substrate-reducing activity and/or the product profile were altered upon substitution of the cofactor in the same protein scaffold, suggesting a fine-tuning effect of the heterometal on the catalytic properties of the cofactor.

Other than the heterometal, the organic compound of the cofactor—which is proposed to function in proton delivery during catalysis—was shown to have an impact on the substrate-reducing profile of nitrogenase. Found in both M- and V-clusters as the organic ligand coordinating the heterometal, homocitrate is synthesized *in vivo* by the *nifV*-encoded homocitrate synthase (NifV), which only generates the (*R*)-homocitrate isomer in the cell.[15,16] Deletion of *nifV* in *Klebsiella pneumoniae* results in the expression of a Mo-nitrogenase variant that contains a citrate-substituted M-cluster analog at the cofactor site of its catalytic MoFe protein component.[17,18] This *K. pneumoniae* Mo-nitrogenase variant shows only 7% N_2-reduction activity as compared to that of its wildtype counterpart and, contrary to the wildtype enzyme, its H_2-evolution activity is inhibited by CO.[19,20] Interestingly, these features seem to resemble those of the wildtype V-nitrogenase, which shows reduced N_2-reducing activity compared to its Mo counterpart,

as well as inhibition of H_2-evolution by CO due to a shift of electrons from H^+-reduction toward CO reduction.

The fact that citrate substitution alters the reactivity of Mo-nitrogenase toward that of the V-nitrogenase makes it tempting for us to generate a V-nitrogenase variant with the same substitution and see how it impacts the reactivity *vice versa*, particularly given the disparate activities of these two homologous nitrogenases toward N_2 and CO. Studies along this line are important as they could provide a tool for fine-tuning the reactivity of the nitrogenase enzyme toward formation of the desired products while offering mechanistic insights into the complex reactions catalyzed by this enzyme. Here, we present a combined biochemical and spectroscopic characterization of a V-nitrogenase variant expressed in a *nifV*-deletion strain of *Azotobacter vinelandii*. Our data reveal an $\alpha\beta_2(\delta)$ subunit composition of its VFe protein component, as well as the presence of a citrate-substituted V-cluster analog in this VFe protein variant.

While the activities of this variant are comparable with those of its wildtype counterpart in N_2- and CO-reduction, there is a clear shift from H_2-evolution toward NH_3-formation in the case of the former and a shift in the opposite direction from CO-reduction toward H_2-evolution in the case of the latter. These observations are consistent with a role of the organic ligand of the cofactor in proton delivery, but more importantly, they point to the possibility of improving ammonia synthesis through modification of this ligand—alone or in combination with variation of other key components of the cofactor. Furthermore, the disparate effects of citrate substitution on the reactivity of nitrogenase toward different substrates imply different reaction sites and/or mechanisms employed by

this enzyme for catalysis, which could be further explored to shed light on the mechanistic details of nitrogenase.

3.3 Results

Taking after the strategy applied to *K. pneumoniae*, a *nif*V deletion strain of *A. vinelandii* was constructed, which expressed a His-tagged VFe protein under N_2-fixing conditions.[20] As indicated by SDS-PAGE, the VFe protein isolated from this *A. vinelandii* strain (designated VnfDGK^{Cit})—contrary to the $\alpha_2\beta_2\delta_2$ wildtype VFe protein (designated VnfDGK)—contains the α- and β-subunits at a molar ratio of 1:2, with the small δ-subunit present in a substoichiometric amount (Figure 3.1A). Such an $\alpha\beta_2$ subunit composition was reported for one of the two species (*i.e.*, $\alpha\beta_2$, $\alpha_2\beta_2$) in an earlier preparation of the non-tagged, wildtype VFe protein from *A. vinelandii*, which was proposed to have one 8Fe P*-cluster ([Fe_8S_7]) at the α/β-subunit interface and one 4Fe unit ([Fe_4S_4]) in the 'orphaned' β-subunit.[21] Interestingly, the metal content of our VnfDGK^{Cit} is consistent with the same assignment as that in the previous report for the P*-cluster-related species (*i.e.*, one 8Fe- and one 4Fe-species) at 100% occupancy, along with a V-cluster-related species (*i.e.*, one 1V/7Fe species) at 50% occupancy (Figure 3.1B). GC-MS analysis further reveals the presence of a citrate-substituted V-cluster analog (designated V-cluster^{Cit}) on VnfDGKCit, showing the presence of citrate and absence of homocitrate in this cofactor species (Figure 3.1C). These results were confirmed by GC retention time (Figure 3.1C) and by the resulting MS fragmentation patterns (Supplementary Figures 3.1-4). Together, these results lead to the proposal of VnfDGK^{Cit} as an $\alpha\beta_2(\delta)$ multimer containing one catalytically functional αβ-dimer with a pair of P*-cluster and V-cluster^{Cit},

as well as a β-subunit carrying a 4Fe cluster as one precursor unit required for the assembly of a complete, 8Fe P*-cluster (Figure 3.1D).

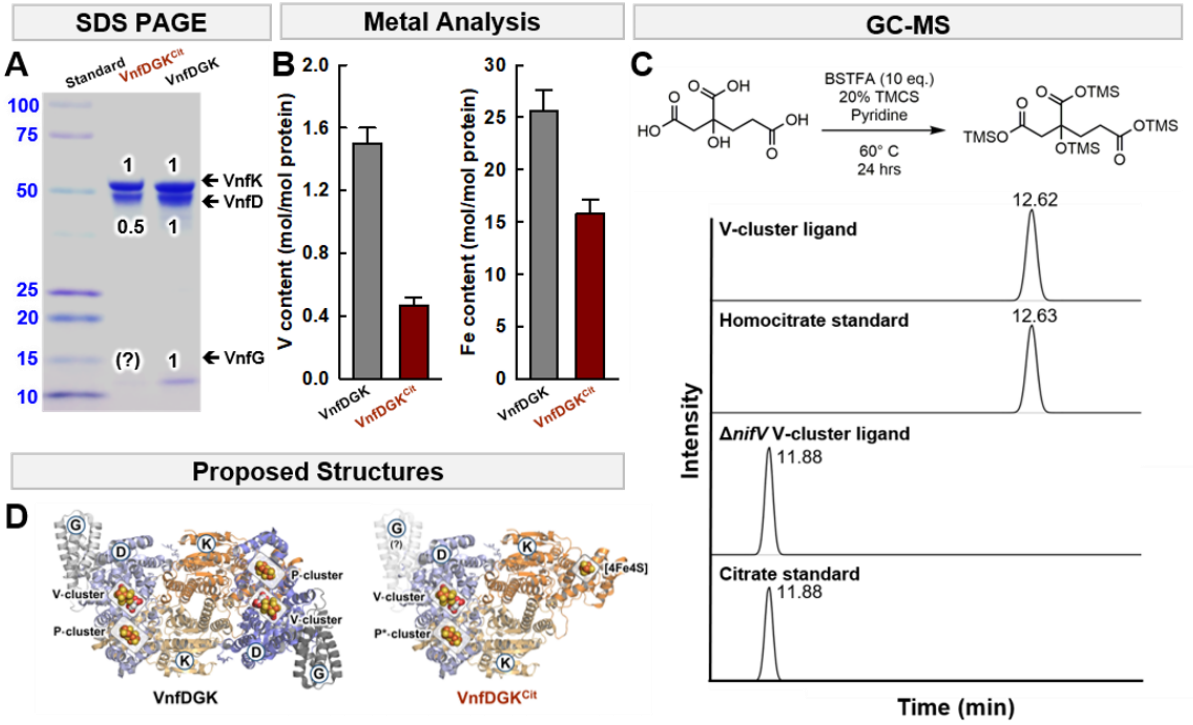

Figure 3.1: Subunit, metal, and organic ligand compositions of VnfDGK^{Cit}. (**A**) SDS-PAGE analysis of VnfDGK and VnfDGK^{Cit}. The molecular masses (in kilodaltons) of the protein standards are shown to the left of the gel, and the subunits are indicated to the right of the gel. (**B**) Metal content of VnfDGK and VnfDGK^{Cit}. Shown are the V (*left*) and Fe (*right*) content of VnfDGK (*gray*) and VnfDGK^{Cit} (*red*) expressed in mole metal/mole protein. (**C**) Derivatization reaction scheme *(upper)* and GC chromatograms of the resulting products (*lower*) from extracted V-cluster, a homocitrate standard, V-cluster^{Cit}, and a citrate standard. (**D**) Crystal structure of VnfDGK (*left*) and proposed structure of VnfDGK^{Cit} (*right*). Based on subunit, metal, and EPR analyses (see Figures 1A and 2A), the $\alpha\beta_2(\delta)$ VnfDGK^{Cit} is proposed to have a P*-cluster and a V-cluster^{Cit} in the αβ dimer, as well as a $[Fe_4S_4]$ cluster in the lone β-subunit. The atoms of the clusters (shown as spheres) are colored as follows: Fe, orange; S, yellow; O, red; C, light gray; V, dark gray. PyMOL was used to generate this figure (PDB ID: 5N6Y).[11]

EPR analysis of the dithionite-reduced VnfDGK^{Cit} protein provides further insight into the cluster composition of this citrate-substituted form of VFe protein (Figure 3.2). Notably, the cofactor-associated S = 3/2 signal of VnfDGK^{Cit} has features at g = 5.50, 5.35, 4.32 and 3.77 that are analogous to, yet distinct from, those of its native VnfDGK

counterpart (Figure 3.2A, *red trace vs. black trace*), demonstrating an impact of citrate substitution on the electronic properties of the cofactor. Moreover, the *S* = 1/2 signal of VnfDGKCit, unlike that of VnfDGK, reflects the contribution from more than one cluster species (Figure 3.2A, *red trace vs. black trace*). Subtraction of the P*-cluster-associated, *S* = 1/2 signal (*g* = 2.03 and 1.92) of a cofactor-deficient VnfDGK (designated VnfDGK^{apo}) from the *S* = 1/2 signal of VnfDGK^{Cit} results in a rhombic *S* = 1/2 signal (*g* = 2.01, 1.92 and 1.88); conversely, subtraction of this rhombic signal from the *S* = 1/2 signal of VnfDGK^{Cit} results in a signal identical to that associated with the P*-cluster (Figure 3.2A, *insets I, II*).[22] The integrated signal intensities of the two *S* = 1/2 signals differ in their temperature dependence (Figure 3.2B, *panel I vs. II*), further illustrating the difference in their origins.

Interestingly, both signals were observed in the $\alpha\beta_2$ form of the early VnfDGK preparation, with the rhombic signal assigned to a [Fe_4S_4] cluster.[21] By analogy, a P*-cluster and a [Fe_4S_4] cluster can be assigned to the $\alpha\beta_2(\delta)$- multimeric VnfDGK^{Cit}, with the 8Fe P*-cluster occupying the αβ-dimeric interface and the 4Fe cluster attached to the lone β-subunit. It is important to note that the *S* = 1/2 signal (*g* = 2.03 and 1.92) of the wildtype VnfDGK shows the same temperature dependency as the P*-cluster of the cofactor-deficient VnfDGK^{apo} and the P*-cluster of the citrate-substituted VnfDGK^{Cit} (Figure 3.2B, *panel I*). This observation, in combination with the fact that the temperature dependency of this *S* =1/2 species clearly differs from the cofactor-associated, *S* =3/2 species in VnfDGK or VnfDGK^{Cit} (Figure 3.2B, *panel III vs. IV*), firmly establishes the wildtype VnfDGK has the same P*-cluster as those found in VnfDGK^{apo} and VnfDGK^{Cit}. Given the diamagnetic nature of the reduced P-cluster in the Mo-nitrogenase, the

paramagnetic behavior of the reduced P*-cluster in V-nitrogenase suggests a difference between the structural/redox properties of the two P-cluster species. This argument is supported by an earlier XAS/EXAFS study of the cofactor-deficient VnfDGK^{apo},which suggests that the P*-cluster consists of a [Fe_4S_4]-like cluster pair.[22]

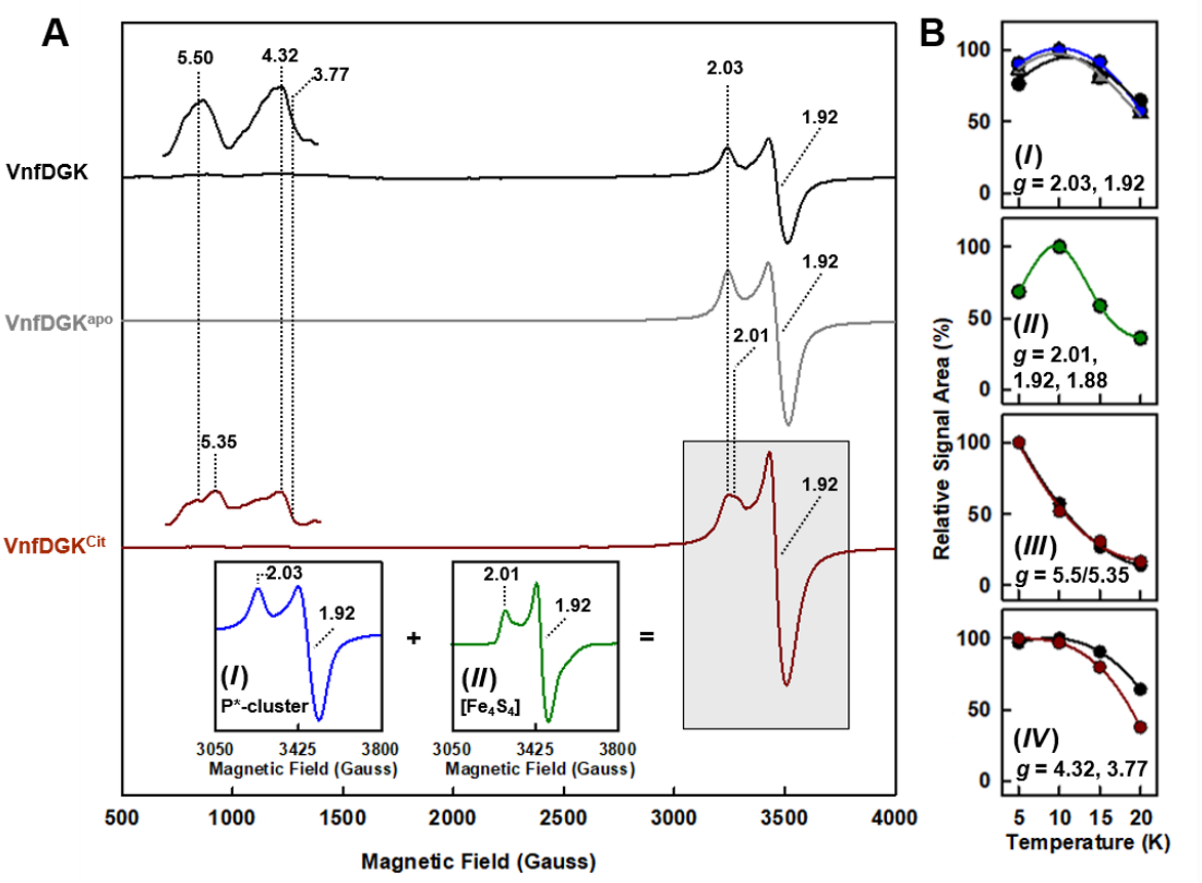

Figure 3.2: Spectroscopic properties of VnfDGK^{Cit}. (**A**) EPR spectra of VnfDGK (*black*), VnfDGK^{apo} (*gray*), and VnfDGK^{Cit} (*red*). The *S* = 3/2 signals in VnfDGK and VnfDGK^{Cit}, which originate from the V-cluster and V-cluster^{Cit}, respectively, are enlarged and shown above the corresponding traces. Insets: *I*, the *S* = 1/2 signal originating from the P*-cluster (*i.e.*, a pair of [Fe_4S_4]-like clusters); *II*, the *S* = 1/2 signal originating from the [Fe_4S_4]$^{+}$-cluster. Note the presence of both the P*-cluster and the [Fe_4S_4] cluster that give rise to the *S* = 1/2 signal in the spectrum of VnfDGK^{Cit}, as well as the presence of the same P*-associated, *S* = 1/2 signal in the spectra of VnfDGK, VnfDGK^{apo}, and VnfDGK^{Cit}. The EPR spectra were collected at 1 mW and 15 K. The *g* values are indicated. (**B**) Temperature dependence of the signal intensity of the *S* = 1/2 species at *g* = 2.03, 1.92 (*I*) and *g* = 2.01, 1.92 (*II*), respectively, and the *S* = 3/2 species at *g* = 5.50, 5.35 (*III*) and *g* = 4.32, 3.77 (*IV*), respectively. The signal intensities are expressed in relative signal areas, with the total signal areas set as 100%. The plots in B are colored the same way as the corresponding EPR traces in A.

Despite the presence of only one catalytically competent αβ-dimer and the alteration of organic compound in it cofactor, the electron flux through VnfDGK^{Cit}—normalized based on the amount of cofactor—is approximately the same as that through VnfDGK when H^+, N_2, C_2H_2, CO or CN^- is supplied as a substrate, suggesting that the previously proposed cooperativity between the two αβ-dimers of nitrogenase during catalysis may not apply to this case (Figure 3.3A).[23] Examination of the product distribution reveals a shift from evolution of H_2 toward formation of NH_3 in the presence of N_2, and a shift in the opposite direction from formation of reduced carbon products toward evolution of H_2 in the presence of carbon substrates, particularly in the cases of CO and CN^- (Figure 3.3B). Among them, the most noteworthy change is perhaps the ~2-fold increase of the molar ratio between NH_3 and H_2 formed from N_2 reduction, as a significant push toward NH_3 formation has not been reported for any nitrogenase variant

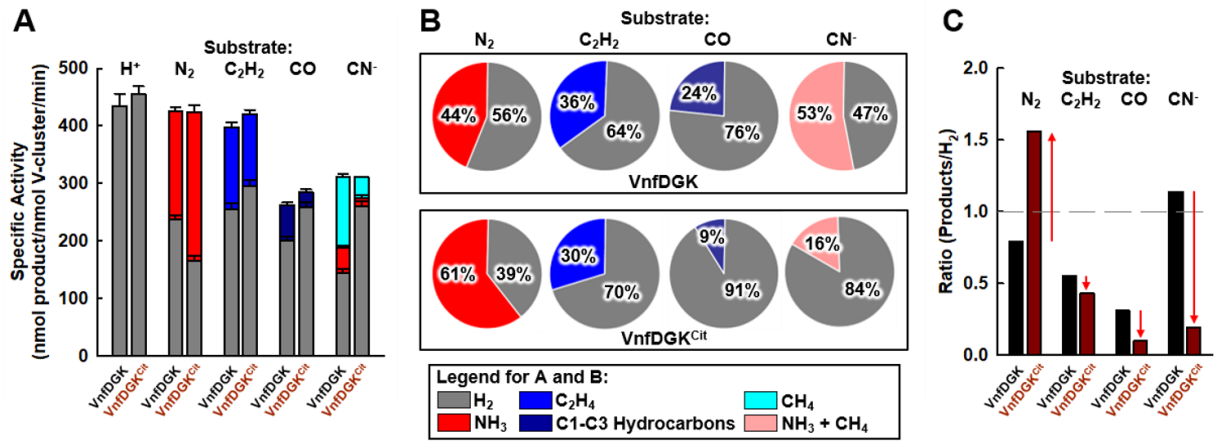

Figure 3.3: Substrate-reducing activities and product profiles of VnfDGK^{Cit}. (**A**) Specific activities of H^+-, N_2-, C_2H_2-, CO- and CN^--reduction by VnfDGK and VnfDGK^{Cit}. Activities are expressed as nmol total electrons in products/nmol cofactor/min. (**B/C**) Product distributions (**B**) and products/H_2 ratios (**C**) of N_2-, C_2H_2-, CO- and CN^--reduction by VnfDGK and VnfDGK^{Cit}. Note that the total electron fluxes are approximately the same in the presence of all substrates tested (**A**), as well as a shift toward NH_3-formation under N_2 and an opposite shift toward H_2-evolution under C_2H_2, CO and CN^- (**C**).

so far. Moreover, the increased N_2-reducing activity of VnfDGK^{Cit} is accompanied by a substantially decreased CO-reducing activity, rendering this citrate-substituted V-nitrogenase similar to the wildtype Mo-nitrogenase in their catalytic behaviors. Taken together, the impact of citrate substitution on H_2-evolution that accompanies N_2- or CO-reduction is consistent with the previously suggested role of homocitrate in assisting proto delivery for substrate reduction by nitrogenase.[24]

3.4 Discussion

The observation of an $\alpha\beta_2(\delta)$ composition of VnfDGK^{Cit} is interesting in that it adds another example of an $\alpha\beta_2$ species that is derived from the $\alpha_2\beta_2$-tetrameric core of the relatively unstable nitrogenase variants (*e.g.*, cofactor-deficient Mo- or V nitrogenase) or produced after multi-step purification procedures of fragile nitrogenase proteins (*e.g.*, non-tagged wildtype V-nitrogenase).[21,22] The conversion of the $\alpha_2\beta_2$ core to an $\alpha\beta_2$ species is consistent with the crystallographic structures of the catalytic components of both Mo- and V-nitrogenases, which shows a structural arrangement of subunits as αββα—in other words, the two β-subunits closely interact with each other, whereas the α subunits bind to the adjacent β-subunits but do not interact with each other.[7,11] Thus, it is not that surprising that one of the α-subunits can easily dissociate from the $\alpha_2\beta_2$ core, leaving behind the $\alpha\beta_2$ species. But conversely, the consistent observation of an incomplete $\alpha\beta_2$ species in the cases of Mo- and V-nitrogenases could have some bearing on the assembly mechanism of the $\alpha_2\beta_2$ tetramer, as it implies that the tetrameric core assembly is initiated with the formation of a β_2 dimer, followed by the attachment of two α-subunits—one at a time—to the respective β-subunit that gives rise to two αβ dimers in a sequential fashion. Completion of one αβ dimer seems to be a prerequisite for the

assembly of the second αβ dimer, as the incomplete $\alpha\beta_2$ form is generated as the predominant species if the cofactor is completely absent from (*e.g.*, $VnfDGK^{apo}$) or partially present at (*e.g.*, $VnfDGK^{Cit}$) the cofactor site.

The partial occupancy (~50%) of the citrate-substituted cofactor species in V-nitrogenase is consistent with the crystallographic observation of a partial occupancy of the citrate-substituted cofactor species in Mo-nitrogenase. In the case of the latter, the crystal structure of the citrate-substituted protein was modelled with partial-occupancy citrate interacting with protein residues surrounding the cofactor via partial-occupancy water molecules.[18] The incomplete incorporation of the citrate-substituted cofactor was attributed to a looser binding of citrate to the cofactor, as *in vitro* studies of cofactor biosynthesis demonstrated a 100-fold stronger preference for homocitrate than that for citrate.[25] Given that *α*-ketoglutarate—an intermediate of the citric acid cycle—is used as a substrate for the synthesis of homocitrate, the preference of homocitrate over citrate for the nitrogenase cofactor synthesis could have implications in the overall metabolic regulation of the nitrogen-fixing organisms. Moreover, the specific requirement of the (*R*)-homocitrate isomer may imply a stereospecific involvement of this organic ligand in nitrogenase catalysis. The differential effects of citrate substitution on the activities of V-nitrogenase in N_2- and CO-reduction seems to support this argument, particularly considering that N_2 and CO are non-competitive inhibitors of each other and may utilize different sites/mechanisms of the cofactor for reduction. It is possible that citrate substitution perturbs proton delivery to these sites differently, favoring one while suppressing the other in a reciprocated manner. In support of this proposal, previous DFT calculations suggested the presence of multiple water/proton chains leading from the

protein surface to the cofactor site, which could participate in different substrate reduction reactions by nitrogenase.[26] While details of this proposal are yet to be elucidated, it does not seem unusual for nitrogenase to utilize more than one site for substrate binding, and substitution of the organic ligand seems to be able to uncouple these events via differential perturbations of proton delivery required for these events.[27–30] As such, results of this study provide a useful tool for further investigation into the reaction mechanism of the enigmatic nitrogenase enzyme. Furthermore, the altered NH_3/H_2 or hydrocarbon/H_2 ratio upon citrate substitution points to the possibility of developing strategies to modify the organic ligand—alone or in combination with variations of other key components of the cofactor—for improved ammonia or hydrocarbon synthesis by nitrogenase or its mimics in the future.

3.5 Materials and Methods

3.5.1 Strain construction and cell growth: *Azotobacter vinelandii* strain YM68A, which expresses a His-tagged form of wildtype VnfDGK in a *nifHDK*-deletion background was used to construct a *nifV*-deletion strain.[12] Specifically, using a previously described protocol, a DNA fragment carrying a 1.3-kb kanamycin resistance cartridge between the flanking sequences of *nifV* on the chromosome of *A. vinelandii* was transformed into YM68A and used to replace *nifV* with the kanamycin resistance cassette via homologous recombination.[31] The resulting *A. vinelandii* strain, designated YM80A, expresses a His-tagged, citrate-substituted variant of VnfDGK (VnfDGK^{Cit}) due to the absence of the *nifV*-encoded homocitrate synthase. Strains YM68A, YM80A and YM7A, which express His-tagged VnfDGK, VnfDGK^{Cit} and VnfDGK^{apo}, respectively, were grown in 180 L batches in a 200 L New Brunswick fermenter (New Brunswick Scientific) in Burke's minimal medium supplemented with 2 mM ammonium acetate as described earlier.[12,22,32] Cells were harvested in the late exponential phase by a flow-through centrifugal harvester (Cepa), and the cell paste was washed with a buffer containing 50 mM Tris-HCl (pH 8.0). Published methods were then used for the purification of His-tagged VnfDGK proteins and non-tagged VnfH.[12,15]

3.5.2 Protein characterization: The subunit compositions of His-tagged VnfDGK and VnfDGK^{Cit} proteins were determined by SDS-PAGE analysis on a 4-20% precast Tris-glycine gel (Bio-Rad). The metal contents of the proteins were determined by inductively coupled plasma-optical emission spectroscopy (ICP-OES) based on previously established protocols.[33]

3.5.3 Cofactor extraction: Cofactor samples were extracted from 1 g of purified VnfDGK or Δ*nifV* VnfDGK, respectively, according to previously published methods.[34] However, dilute (75 mM) HCl was used to precipitate the protein samples in lieu of dilute citric acid. In short, proteins were purified by affinity chromatography. Glycerol and imidazole were removed from the protein samples such that the resulting protein solution contained 5 mg/mL of protein, 25 mM Tris (pH 8), and 2 mM DT. Protein was precipitated by titration to pH 5.5 with 75 mM HCl. V-cluster or V-cluster^{Cit} were extracted twice from the solution with DMF. Cofactors were then extracted in NMF with 4 mM 1,4-benzenedithiol and concentrated under reduced pressure.

3.5.4 Organic acid determination: Extracted cofactor samples were exposed to air for 4 hours, evaporated to dryness under Ar, and re-suspended in pyridine prior to incubation at 70°C for 14 h under Ar with bis-(trimethylsilyl) trifluoroacetamide (BSTFA) and 30% trimethylchlorosilane (TMCS). BSTFA, in combination with TMCS, convert alcohol functional groups to trimethylsilyl (TMS) groups. The derivatized products were then extracted with oxygen-free hexanes prior to being analyzed by GC-MS. For GC-MS analysis, 1 μL of the hexane extraction layer was injected into a GC-MS (Thermo Scientific, Trace 1300 GC and ISQ single quadrupole MS) with a split injector set at 120°C. The flow rate of high purity He carrier gas was set at 12 mL/min with a split ratio of 2. A 4 mm ID liner with glass wool was used to protect the column from unreacted silylating reagent and inorganic components of the derivatization reaction mixture. Derivatized products were separated on a VF-5ms 30 m x 0.25 mm capillary column (Agilent Technologies), which was held at 120°C for 3 min, heated to 200°C at a rate of 10°C/min, and held at 200°C for another 19 min. The mass spectrometer was operated

in electron impact (EI) ionization and positive ion modes. Silylated products were identified by using both the scan mode and the selected ion monitoring (SIM) mode of GC-MS.

3.5.5 EPR spectroscopy: EPR samples were prepared in a Vacuum Atmospheres dry box at an oxygen level of <4 ppm. All samples contained 25 mM Tris-HCl (pH 8.0), 10% glycerol and 2 mM sodium dithionite ($Na_2S_2O_4$). The EPR spectra were taken in perpendicular mode using a Bruker ESP 300 Ez spectrophotometer (Bruker) interfaced with an Oxford Instruments ESR-9002 liquid helium continuous flow cryostat. All spectra were recorded at various temperatures as indicated in Figure 3.2 using a microwave power of 20 mW, a gain of $5x10^4$, a modulation frequency of 100 kHz, and a modulation amplitude of 5 G. A microwave frequency of 9.62 GHz was used to collect five scans for each sample.

3.5.6 Activity assays: All nitrogenase activity assays were carried out as described earlier[31,34] except for the cyanide assay, where 5 mM of sodium cyanide (NaCN) was added to the reaction mixture under Ar prior to the addition of protein components.[31,35] The hydrocarbon products were analyzed as described elsewhere.[2,3,33] Ammonium was determined by a high performance liquid chromatography fluorescence method, and

hydrogen was analyzed as described previously.[36,37]

3.6 Supplementary Information

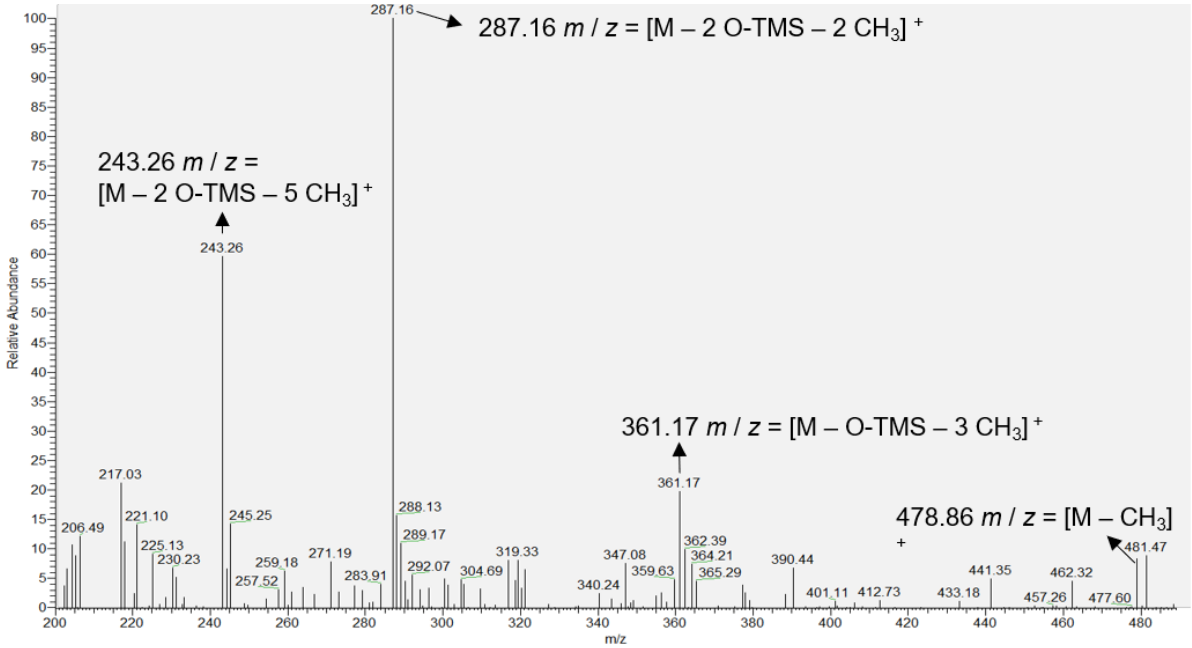

Supplementary Figure 3.1: Mass spectrometry fragments (EI) for BSTFA-derivatized VnfDGK V-cluster organic ligand at RT = 12.62 min. Mass of fully derivatized homocitrate [M⁺] is 494 *m* / *z*. Parent ion is [M⁺ - 207] (287 *m* / *z*), which is expected for BSTFA derivatives.[38,39]

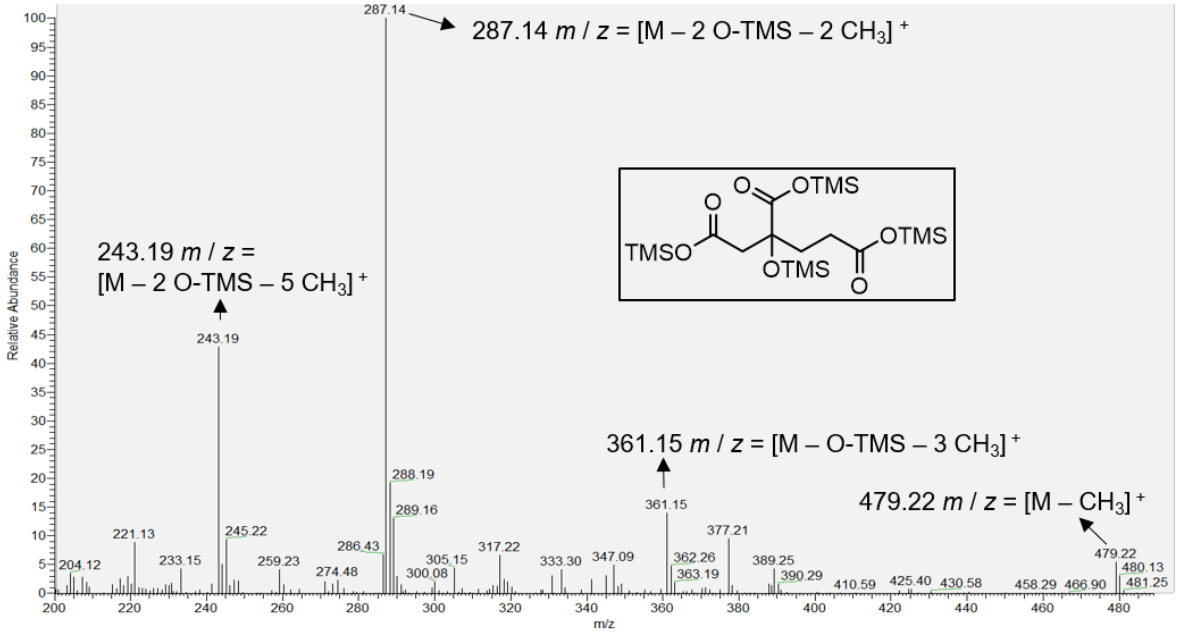

Supplementary Figure 3.2: Mass spectrometry fragments (EI) for BSTFA-derivatized homocitrate standard (inset, boxed) at RT = 12.63 min. Mass of fully derivatized homocitrate [M⁺] is 494 *m* / *z*. Parent ion is [M⁺ - 207] (287 *m* / *z*), which is expected for BSTFA derivatives.[38,39]

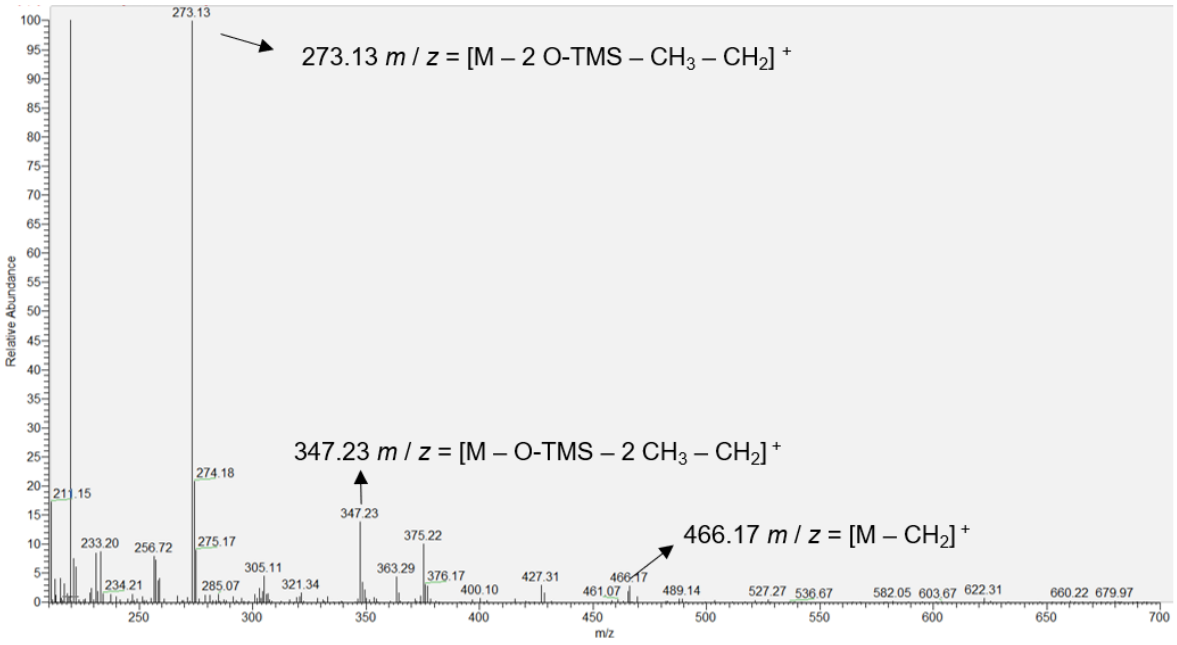

Supplementary Figure 3.3: Mass spectrometry fragments (EI) for BSTFA-derivatized Δ*nifV* VnfDGK V-cluster (V-cluster^{Cit}) organic ligand at RT = 11.88 min. Mass of fully derivatized citrate [M^+] is 480 *m* / *z*. Largest ion observed is [M^+ - 207] (273 *m* / *z*), which is expected for BSTFA derivatives.[38,39]

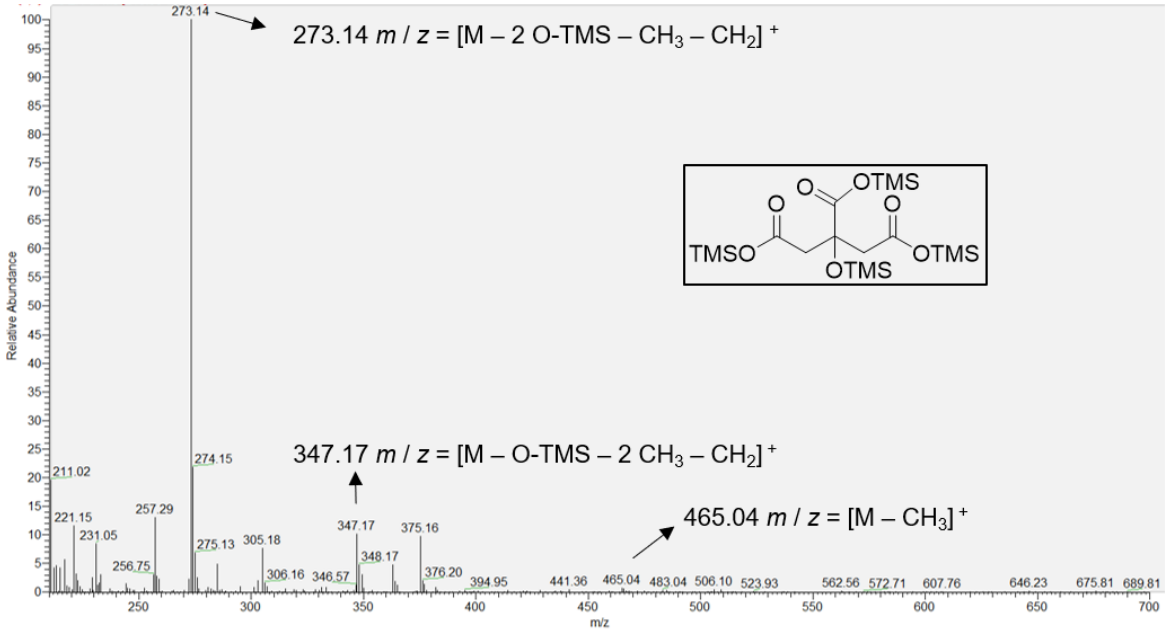

Supplementary Figure 3.4: Mass spectrometry fragments (EI) for BSTFA-derivatized citrate standard (inset, boxed) at RT = 11.88 min. Mass of fully derivatized citrate [M^+] is 480 *m* / *z*. Largest ion observed is [M^+ - 207] (273 *m* / *z*), which is expected for BSTFA derivatives.[38,39]

3.7 References

(1) Burgess, B. K.; Lowe, D. J. *Chem. Rev.* **1996**, *96* (7), 2983–3012.

(2) Lee, C. C.; Hu, Y.; Ribbe, M. W. *Science* **2010**, *329* (5992), 642.

(3) Hu, Y.; Lee, C. C.; Ribbe, M. W. *Science* **2011**, *333* (6043), 753–755.

(4) Rofer-DePoorter, C. K. *Chem. Rev.* **1981**, *81* (5), 447–474.

(5) Lee, C. C.; Hu, Y.; Ribbe, M. W. *Angew. Chem. Int. Ed.* **2011**, *50* (24), 5545–5547.

(6) Eady, R. R. *Chem. Rev.* **1996**, *96* (7), 3013–3030.

(7) Rees, D. C.; Tezcan, F. A.; Haynes, C. A.; Walton, M. Y.; Andrade, S.; Einsle, O.; Howard, J. B. *Philos. Trans. Royal Soc. A* **2005**, *363* (1829), 971–984.

(8) Hoffman, B. M.; Lukoyanov, D.; Yang, Z. Y.; Dean, D. R.; Seefeldt, L. C. *Chem. Rev.* **2014**, *114* (8), 4041–4062.

(9) Hu, Y.; Ribbe, M. W. *J. Biol. Inorg. Chem.* **2015**, *20* (2), 435–445.

(10) Hu, Y.; Ribbe, M. W. *Annu. Rev. Biochem.* **2016**, *85* (1), 455–483.

(11) Sippel, D.; Einsle, O. *Nat. Chem. Biol.* **2017**, *13* (9), 956–960.

(12) Lee, C. C.; Hu, Y.; Ribbe, M. W. *Proc. Natl. Acad. Sci.* **2009**, *106* (23), 9209–9214.

(13) Rebelein, J. G.; Lee, C. C.; Newcomb, M.; Hu, Y.; Ribbe, M. W. *MBio* **2018**, *9* (2).

(14) Lee, C. C.; Tanifuji, K.; Newcomb, M.; Liedtke, J.; Hu, Y.; Ribbe, M. W. *ChemBioChem* **2018**, *19* (7).

(15) Zheng, L.; White, R. H.; Dean, D. R. *J. Bacteriol.* **1997**, *179* (18), 5963–5966.

(16) Hoover, T. R.; Robertson, A. D.; Cerny, R. L.; Hayes, R. N.; Imperial, J.; Shah, V. K.; Ludden, P. W. *Nature* **1987**, *329* (6142), 855–857.

(17) Liang, J.; Madden, M.; Shah, V. K.; Burris, R. H. *Biochemistry* **1990**, *29* (37), 8577–8581.

(18) Mayer, S. M.; Gormal, C. A.; Smith, B. E.; Lawson, D. M. *J. Biol. Chem.* **2002**, *277* (38), 35263–35266.

(19) McLean, P. A.; Dixon, R. A. *Nature* **1981**, *292* (5824), 655–656.

(20) McLean, P. A.; Smith, B. E.; Dixon, R. A. *Biochem. J.* **1983**, *211* (3), 589–597.

(21) Blanchard, C. Z.; Hales, B. J. *Biochemistry* **1996**, *35* (2), 472–478.

(22) Hu, Y.; Corbett, M. C.; Fay, A. W.; Webber, J. A.; Hedman, B.; Hodgson, K. O.; Ribbe, M. W. *Proc. Natl. Acad. Sci.* **2005**, *102* (39), 13825–13830.

(23) Danyal, K.; Shaw, S.; Page, T. R.; Duval, S.; Horitani, M.; Marts, A. R.; Lukoyanov, D.; Dean, D. R.; Raugei, S.; Hoffman, B. M.; Seefeldt, L. C.; Antony, E. *Proc. Natl. Acad. Sci.* **2016**, *113* (40), E5783–E5791.

(24) Demadis, K. D.; Malinak, S. M.; Coucouvanis, D. *Inorg. Chem.* **1996**, *35* (13), 4038–4046.

(25) Hoover, T. R.; Shah, V. K.; Roberts, G. P.; Ludden, P. W. *J. Bacteriol.* **1986**, *167* (3), 999–1003.

(26) Dance, I. *Dalt. Trans.* **2012**, *41* (25), 7647–7659.

(27) Pollock, R. C.; Orme-Johnson, W. H.; Lee, H. I.; DeRose, V. J.; Hoffman, B. M.; Cameron, L. M.; Hales, B. J. *J. Am. Chem. Soc.* **1995**, *117* (33), 8686–8687.

(28) Lee, H. I.; Cameron, L. M.; Hales, B. J.; Hoffman, B. M. *J. Am. Chem. Soc.* **1997**, *119* (42), 10121–10126.

(29) George, S. J.; Ashby, G. A.; Wharton, C. W.; Thorneley, R. N. F. *J. Am. Chem. Soc.* **1997**, *119* (27), 6450–6451.

(30) Christiansen, J.; Seefeldt, L. C.; Dean, D. R. *J. Biol. Chem.* **2000**, *275* (46), 36104–36107.

(31) Hu, Y.; Fay, A. W.; Dos Santos, P. C.; Naderi, F.; Ribbe, M. W. *J. Biol. Chem.* **2004**, *279* (52), 54963–54971.

(32) Hu, Y.; Fay, A. W.; Schmid, B.; Makar, B.; Ribbe, M. W. *J. Biol. Chem.* **2006**, *281* (41), 30534–30541.

(33) Sickerman, N. S.; Tanifuji, K.; Lee, C. C.; Ohki, Y.; Tatsumi, K.; Ribbe, M. W.; Hu, Y. *J. Am. Chem. Soc.* **2017**, *139* (2), 603–606.

(34) Fay, A. W.; Blank, M. A.; Lee, C. C.; Hu, Y.; Hodgson, K. O.; Hedman, B.; Ribbe, M. W. *J. Am. Chem. Soc.* **2010**, *132* (36), 12612–12618.

(35) Burgess, B. K.; Jacobs, D. B.; Stiefel, E. I. *Biochim. Biophys. Acta* **1980**, *614* (1), 196–209.

(36) Corbin, J. L. *Appl. Environ. Microbiol.* **1984**, *47* (5), 1027–1030.

(37) Gavini, N.; Burgess, B. K. *J. Biol. Chem.* **1992**, *267* (29), 21179–21186.

(38) Kowalewski, K.; Gierczak, T. *J. Chromatogr. A* **2011**, *1218* (41), 7264–7274.

(39) Schiller, M.; Von Der Heydt, H.; März, F.; Schmidt, P. C. *J. Chromatogr. A* **2002**, *968* (1–2), 101–111.

Chapter 4:

Characterization of a V-nitrogenase variant from *Azotobacter vinelandii* that contains a citrate-substituted cofactor

4.1 Abstract

Nitrogenase catalyzes the reduction of N_2 at its active site cofactor. In previous studies, we presented characterization of a V-nitrogenase Δ*nifV* mutant from *Azotobacter vinelandii* that contained a citrate-substituted cofactor (VnfDGK^{Cit}). In this work, we present biochemical and spectroscopic characterization of the isolated citrate-substituted V-cluster (V-cluster^{Cit}). V-cluster^{Cit} was extracted from the VnfDGK^{Cit} protein scaffold and used to reconstitute a cofactor-deficient Mo-nitrogenase (apo-NifDK). Substrate reduction by this reconstituted protein generally mirrors patterns observed with the whole protein experiments discussed in Chapter 3. As in the whole protein study, the citrate-substituted cofactor causes a shift of N_2-reduction from H_2-evolution toward NH_3-formation. The observed shift toward NH_3 production from N_2 confirms that altering the V-cluster organic ligand can tune nitrogenase reactivity and the resulting product profile. These finding can be used to inform future studies that aim to improve biological nitrogen fixation using nitrogenase mutants or mimics.

4.2 Introduction

Vanadium nitrogenase (V-nitrogenase) catalyzes the reduction of various substrates, including N_2, carbon monoxide (CO), acetylene (C_2H_2), and protons (H^+). These reductions require both catalytic and reductase proteins to facilitate electron transfer through multiple metal cofactors. Reduction occurs at the active site cofactor of V-nitrogenase (V-cluster [(*R*)-homocitrate VFe_7S_8C], figure 5.1). The V-cluster contains an organic (*R*)-homocitrate ligand coordinated to the vanadium atom. The exact purpose of this organic ligand is unknown, but it essential for nitrogenase activity, and altering the organic ligand can significantly alter nitrogenase reactivity.[1–5]

One hypothesis for the role of the ligand in catalysis is that (*R*)-homocitrate may facilitate the shuttling of protons towards the nitrogenase active site.[3,6] Within the cell, (*R*)-homocitrate is synthesized by the homocitrate synthase NifV, and earlier work with *Klebsiella pneumoniae* (*K. pneumoniae*) characterized a Δ*nifV* mutant and the resulting influences on the molybdenum nitrogenase (Mo-nitrogenase).[7,8] The Δ*nifV* Mo-nitrogenase in *K. pneumoniae* utilized citrate as the organic ligand for the catalytic cofactor in the absence of (*R*)-homocitrate. These citrate-containing mutants demonstrated very low activities in terms of N_2, C_2H_2, and H^+ reduction.[9–11]

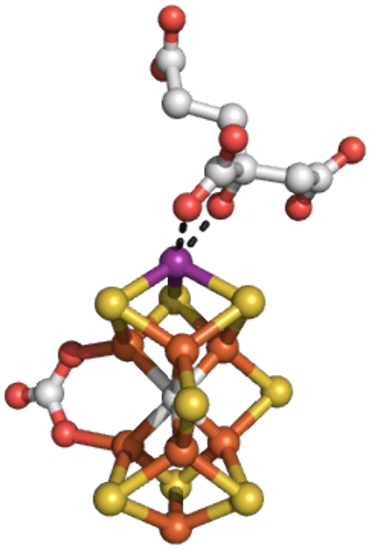

Figure 4.1: V-cluster from wildtype V-nitrogenase. A molecule of (*R*)-homocitrate is coordinated to the vanadium atom. Color codes: purple, vanadium; yellow, sulfur; orange, iron; gray, carbon; red, oxygen. From PDB 5N6Y.

In Chapter 3 of this thesis, a Δ*nifV* mutant was created in a V-nitrogenase-expressing *A. vinelandii* cell line for the first time. The V-cluster from this mutant was extracted, and the ligand was identified as citrate by gas chromatography with mass spectrometry (GC-MS) analysis (Figure 3.1C on page 52). The Δ*nifV* mutant ($VnfDGK^{Cit}$) was compared to the wildtype V-nitrogenase (VnfDGK) in assays utilizing N_2, CO, C_2H_2, and H^+ as substrates. In these whole protein studies, the $VnfDGK^{Cit}$ protein is similar to VnfDGK in terms of the production of C_2H_4 from C_2H_2 and H_2 from H^+. Interestingly, $VnfDGK^{Cit}$ shows a shift of N_2-reduction from H_2-evolution toward NH_3-formation (Figure

3.3 on page 56). This is the first nitrogenase mutant that shows an increased ratio of NH_3 production from N_2.

The altered ligand is likely a large factor in the altered reactivity profile of VnfDGK^{Cit}. Citrate is smaller than (*R*)-homocitrate, and the shortened ligand likely decreases protein shuttling towards at least one substrate binding site, which causes reduced H_2 formation in the presence of N_2 substrate. The lack of influence on the production of H_2 from H^+ suggests that H_2 formation from H^+ and H_2 formation during N_2 turnover occur at two different sites on the V-cluster or within the VnfDGK protein. However, it is unclear whether the organic ligand is the only contributor to the observed differences discussed in Chapter 3. SDS-PAGE and inductively coupled plasma-optical emission spectroscopy (ICP-OES) analyses of the purified VnfDGK^{Cit} indicated that it has an altered protein subunit composition (Figure 3.1 on page 52). Unlike the wildtype VnfDGK, which has a subunit composition of $\alpha_2\beta_2\delta_2$, VnfDGK^{Cit} has a composition that appears to be $\alpha\beta_2$ with a small amount of δ ($\alpha\beta_2(\delta)$). Due to this major structural difference, it is unclear whether the altered cofactor ligand or the altered protein structure are equal contributors to the altered reactivity. Therefore, many questions remain regarding the source of the reactivity differences observed in VnfDGK^{Cit}.

To address these questions, the catalytic V-cluster from VnfDGK^{Cit} (designated V-cluster^{Cit}) and the V-cluster from wildtype VnfDGK (designated V-cluster) were extracted from their respective protein scaffolds via previously published methods.[12] The cofactor samples were used to reconstituted a cofactor-deficient Δ*nifB* NifDK mutant (designated apo-NifDK). After normalizing the protein scaffold of the isolated cofactor samples, the

reconstituted proteins were compared in terms of their substrate-reduction capabilities and compared to wildtype VnfDGK.

These experiments align somewhat with patterns observed with the whole protein studies discussed in Chapter 3. V-cluster^{Cit} in apo-NifDK, like VnfDGK^{Cit}, demonstrated a shift of N_2-reduction from H_2-evolution toward NH_3-formation. When in the in apo-NifDK scaffold, V-cluster^{Cit} and V-cluster in produce comparable amounts of C_2H_4 from C_2H_2. However, H_2 production from H^+ is greatly reduced for V-cluster^{Cit} in apo-NifDK, and this trend was not observed with VnfDGK^{Cit}. This difference in H^+ reduction indicates that the protein scaffold plays an important role in this conversion. The results of this work build upon the work discussed in Chapter 3 and validate the previously observed changes in the N_2 reduction product profile. This work provides further input regarding the possibility of tuning nitrogenase reactivity toward formation of ammonia while offering mechanistic insight into catalysis by nitrogenase.

4.3 Results

The VnfDGK protein from a *nifV* deletion strain was expressed and purified from *A. vinelandii*. The wildtype VnfDGK protein and apo-NifDK were also produced and purified using previously published methods.[13] Samples of purified proteins were utilized to extract the respective V-clusters (V-cluster^{Cit} and V-cluster) into NMF using previously reported methods.[12] After cofactor extraction, both samples were analyzed for vanadium concentration using ICP-OES. The concentration of vanadium within the V-cluster^{Cit} sample was found to be 0.694 ± 0.172 mM V and 0.876 ± 0.342 mM V within the V-cluster sample.

The cofactor samples were used to reconstituted apo-NifDK using previously published assay conditions.[14–16] The cofactor extraction solvent (NMF) can cause inhibition of nitrogenase reactivity. Therefore, optimal reconstitution of apo-NifDK and resulting enzymatic activity occurs when small volumes of extracted cofactor are included in the assay mixture (ideally less than 15 μL of NMF within a 700 μL aqueous assay). Enzymatic activity decreases at volumes below and above the ideal cofactor volume. To determine the optimal volume of cofactor to include within reconstitution assays, cofactor titration experiments were performed using C_2H_2 as a substrate. Optimal activity of the apo-NifDK reconstituted with V-cluster (apo + V-cluster) was achieved when 10 μL of extracted cofactor was combined with 0.3 mg of apo-NifDK in a total assay volume of 700 μL. Optimal C_2H_4 production by apo-NifDK reconstituted with V-cluster^{Cit} (apo + V-cluster^{Cit}) was achieved when 14 μL of extracted cofactor was combined with 0.3 mg of apo-NifDK (Figure 4.2). These altered volumes roughly mirror the differences in [V] determined by ICP-OES: the extracted V-cluster is ~1.2-fold as concentrated as V-cluster^{Cit}, and 1.4x as much V-cluster^{Cit} was required to reach its optimal substrate reduction activity.

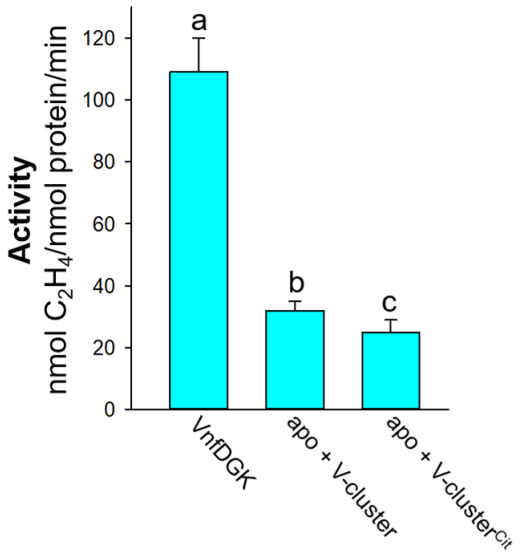

Figure 4.2: Production of C_2H_4 from C_2H_2 by a) wildtype VnfDGK, b) apo-NifDK reconstituted with extracted V-cluster from WT VnfDGK, and c) apo-NifDK reconstituted with extracted V-cluster^{Cit} from Δ*nifV* VnfDGK. Activity is given in nmol product formed/nmol catalytic protein/minute. Error bars are S.D. from n=3.

Cofactor samples were incubated with apo-NifDK prior to initiation of substrate reduction. A VnfDK control was also included for comparison. Samples (VnfDGK, apo + V-cluster, and apo + V-cluster^{Cit}) were first tested for their ability to convert C_2H_2 into C_2H_4. Apo + V-cluster was 29% as active as the WT VnfDGK protein at producing C_2H_4, and apo + V-cluster^{Cit} was 22% as active as VnfDGK (Figure 4.2). The reconstituted proteins did not produce a detectable amount of C_2H_6. This large decrease in activity of reconstituted proteins is expected given the inefficiency of cofactor reconstitution.[12,14–16] The samples were tested for the ability to convert H^+ into H_2 in the absence of substrate. Apo + V-cluster was 58% as active as VnfDGK and apo + V-cluster^{Cit} was 24% as active as VnfDGK (Figure 4.3). The samples were also provided with N_2 substrate. In terms of NH_3 production, apo + V-cluster was 23% as active as VnfDGK and apo + V-cluster^{Cit} was 29% as active as VnfDGK (Figure 4.4, green bars). In terms of H_2 production in the presence of N_2, apo + V-cluster was 32% as active as VnfDGK and apo + V-cluster^{Cit} was 27% as active as VnfDGK (Figure 4.4, gray bars). The samples were also incubated with CO, but no hydrocarbon products were detected for the reconstituted protein samples.

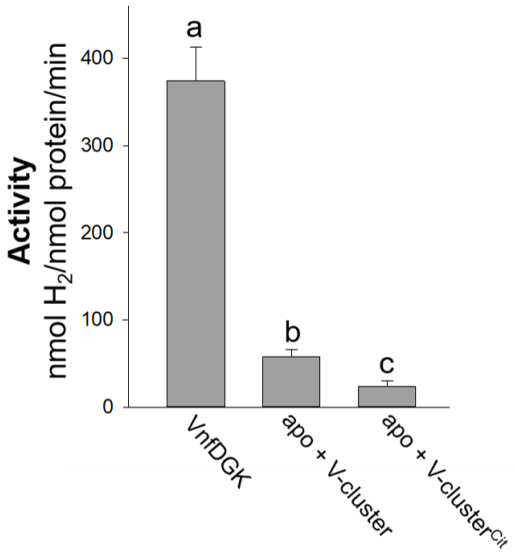

Figure 4.3: Production of H_2 from H^+ by a) wildtype VnfDGK, b) apo-NifDK reconstituted with extracted V-cluster from WT VnfDGK, and c) apo-NifDK reconstituted with extracted V-cluster^{Cit} from Δ*nifV* VnfDGK. Activity is given in nmol product formed/nmol catalytic protein/minute. Error bars are S.D. from n=3.

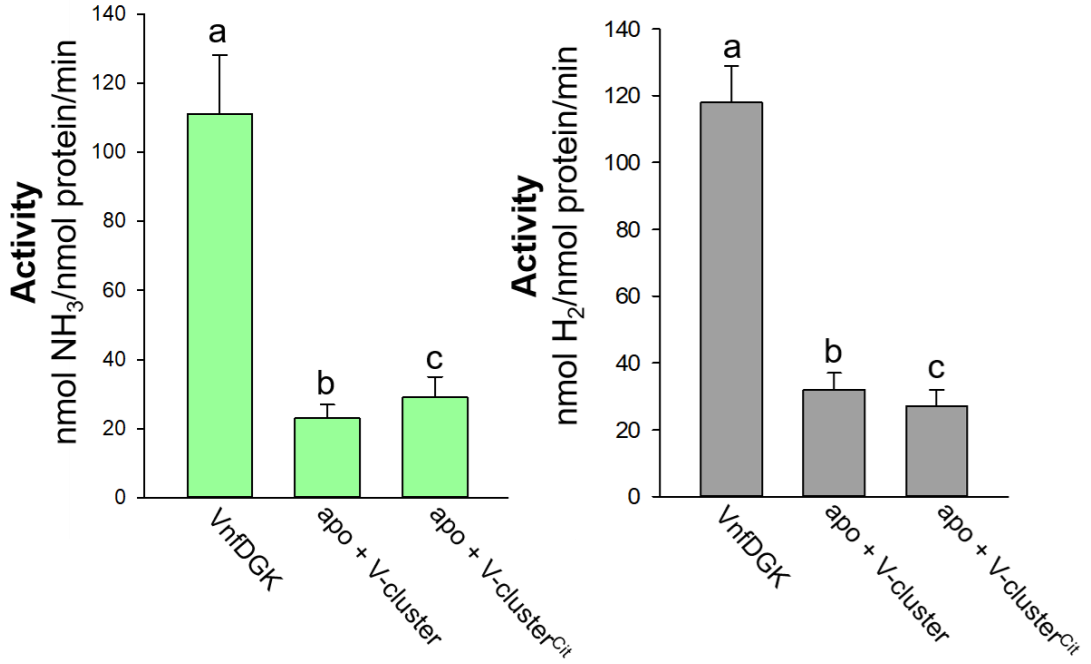

Figure 4.4: Production of NH_3 (green bars, left) and H_2 (gray bars, right) from N_2 by a) wildtype VnfDGK, b) apo-NifDK reconstituted with extracted V-cluster from WT VnfDGK, and c) apo-NifDK reconstituted with extracted V-cluster^{Cit} from Δ*nifV* VnfDGK. Activity is given in nmol product formed/nmol catalytic protein/minute. Error bars are S.D. from n=3.

The extracted cofactor samples were also analyzed using EPR spectroscopy (Figure 4.5). The V-cluster signal was similar to previously-published spectra in which an *S* = 3/2 cofactor-associated signal is observed.[12] The V-cluster^{Cit} shares features with V-cluster, but the intensity of the features is different between the two cofactor samples. Overall, both spectra appear to be *S* = 3/2, although the intricacies of the spectra have not been thoroughly characterized at this time. The intensity of the features between 500 and 3000 Gauss (*g* = 5.88, 5.06, and 3.29 for V-cluster and *g* = 5.92, 5.04, and 3.25 for V-cluster^{Cit}) is lower for the V-cluster^{Cit} spectrum (Figure 4.5B). The magnitude of the feature around 3400 Gauss (*g* = 2.05 for V-cluster and *g* = 2.01 for V-cluster^{Cit}) is much greater in the V-cluster^{Cit} spectrum (Figure 4.5C). This analysis indicates that extracted V-cluster^{Cit} retains the overall *S* = 3/2 signal typically observed for isolated V-cluster.

However, the differences in feature magnitude indicate that altering the organic ligand of the V-cluster influences the electronic properties of the cofactor.

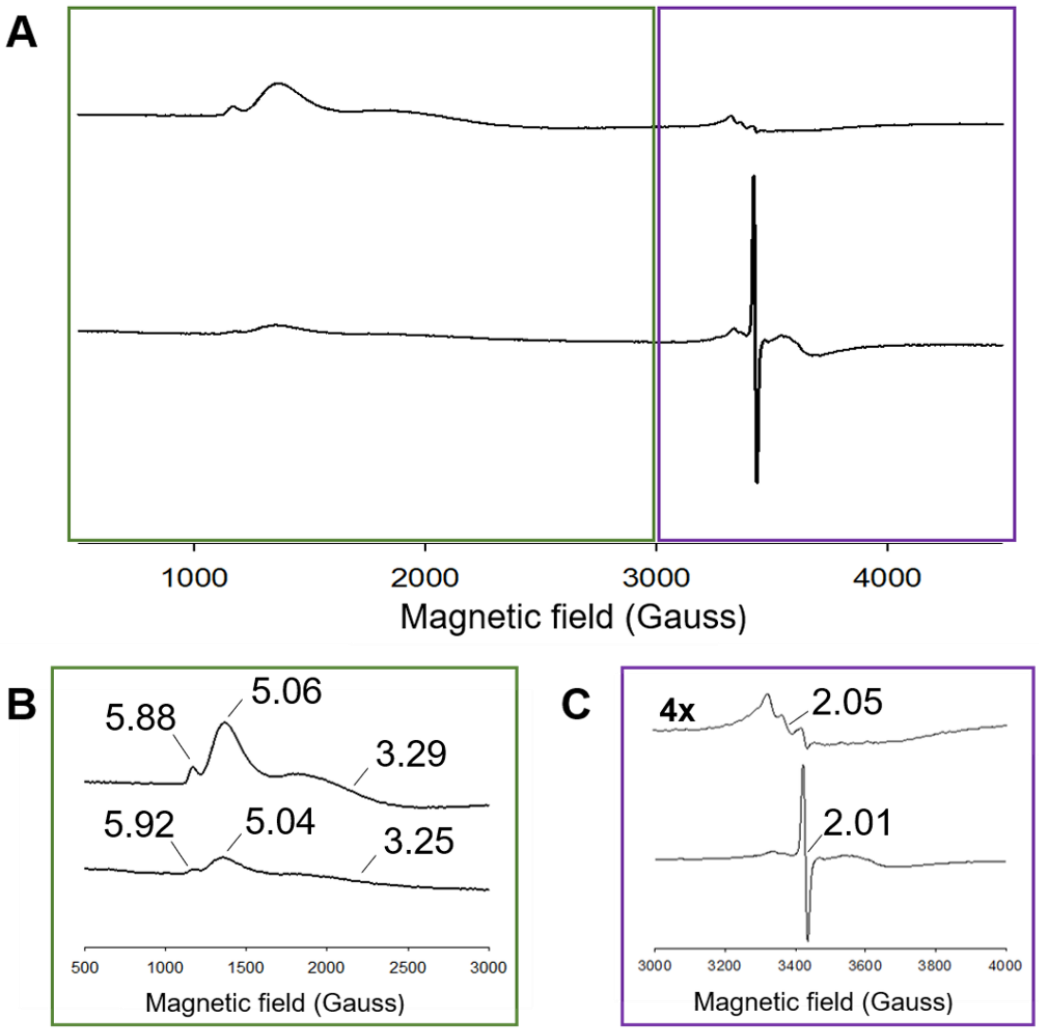

Figure 4.5: EPR spectra of **A)** V-cluster extracted from VnfDGK (upper signal) and V-cluster^{Cit} extracted from Δ*nifV* VnfDGK (lower signal). Detailed views of the 500-3000 Gauss (green box) and 3000-4000 Gauss (purple box) regions are shown in more detail in **B** and **C**, where the V-cluster signal is shown on top and the V-cluster^{Cit} signal is shown on the bottom. Spectra collected at 20 mW and 6 K.

Taken together, these results indicate an overall influence of the cofactor ligand on substrate reduction. The activity trends observed with the isolated cofactors are generally mirrored in the whole protein studies discussed in Chapter 3, which supports the conclusions that the differential reactivities observed in the whole protein studies are a result of the altered organic ligand rather than the incomplete protein subunit composition of VnfDGK^{Cit}.

4.4 Discussion

Using the reactivity and EPR analysis of the extracted V-cluster and V-cluster^{Cit}, it is possible to build upon the results of the whole protein studies discussed in Chapter 3. Similar results were observed with the reconstituted proteins as with the whole protein experiments. The most notable difference between the reconstituted proteins and the whole protein experiments is the marked decrease in H_2 formation from H^+ that was observed with the reconstituted proteins but not in the whole protein studies. For VnfDGK and VnfDGK^{Cit}, H_2 production from H^+ in solution was similar (Figure 3.3A, page 56). However, for apo + V-cluster and apo + V-cluster^{Cit}, apo + V-cluster^{Cit} activity was only 41% of the activity of apo + V-cluster. Placing V-cluster^{Cit} in the NifDK protein scaffold alters the cofactor properties, and therefore the production of H_2 from H^+, in a unique way that was not observed with VnfDGK^{Cit}. The reason behind this difference has not been thoroughly probed at this time, but additional studies with other substrates and products (i.e. the production of H_2 under C_2H_2 and H_2 under CO) may provide valuable insight into this phenomenon

Most interestingly, when provided with N_2 substrate, V-cluster^{Cit} favors production of NH_3 as a product over H_2. This mirrors the activity of VnfDGK^{Cit} and supports the

conclusion that the altered N_2 reduction capabilities of VnfDGK^{Cit} are a result of the citrate ligand. Additional studies are needed to identify what chemical aspects of the organic ligand are the most important in influencing electron and proton flow towards the active site. These results, taken together with the results discussed in Chapter 3, show that altering the organic ligand of the V-cluster provides a useful tool to tune the reactivity and product profile of VnfDGK.

4.5 Materials and methods

4.5.1 Strain construction and cell growth: *Azotobacter vinelandii* strain YM68A, which expresses a His-tagged form of wildtype VnfDGK in a *nifHDK*-deletion background was used to construct a *nifV*-deletion strain.[17] Specifically, using a previously described protocol, a DNA fragment carrying a 1.3-kb kanamycin resistance cartridge between the flanking sequences of *nifV* on the chromosome of *A. vinelandii* was transformed into YM68A and used to replace *nifV* with the kanamycin resistance cassette via homologous recombination.[18] The resulting *A. vinelandii* strain, designated YM80A, expresses a His-tagged, citrate-substituted variant of VnfDGK (VnfDGK^{Cit}) due to the absence of the *nifV*-encoded homocitrate synthase. Strains YM68A, YM80A, which express His-tagged VnfDGK and VnfDGK^{Cit} respectively, were grown in 180 L batches in a 200 L New Brunswick fermenter (New Brunswick Scientific) in Burke's minimal medium supplemented with 2 mM ammonium acetate as described earlier.[17,19,20] Cells were harvested in the late exponential phase by a flow-through centrifugal harvester (Cepa), and the cell paste was washed with a buffer containing 50 mM Tris-HCl (pH 8.0). Published methods were then used for the purification of His-tagged VnfDGK proteins and non-tagged VnfH.[12,15]

4.5.2 Cofactor extraction and analysis: Cofactor samples were extracted from 1 g of purified VnfDGK or Δ*nifV* VnfDGK, respectively, according to previously published methods.[12] However, dilute (75 mM) HCl was used to precipitate the protein samples in lieu of dilute citric acid. In short, proteins were purified by affinity chromatography. Glycerol and imidazole were removed from the protein samples such that the resulting protein solution contained 5 mg/mL of protein, 25 mM Tris (pH 8), and 2 mM DT. Protein

was precipitated by titration to pH 5.5 with 75 mM HCl. V-cluster or V-cluster^{Cit} were extracted twice from the solution with DMF. Cofactors were then extracted in NMF with 4 mM 1,4-benzenedithiol and concentrated under reduced pressure.

For ICP-OES analysis, cluster or protein samples were mixed with 20% HNO_3 and degraded at 250 °C for 15 min. Samples were diluted to 10 mL with pure water. Concentrations of Mo, V, Fe, and S were determined via analysis by ICP-OES (Thermo Scientific iCAP 7000) after calibration with standard solutions of Mo, V, Fe, and S. Ar was used as the plasma gas and N_2 was used as the purge gas.

4.5.3 Activity assays: Reconstitution assays require cofactor samples and apo-NifDK to be combined in the presence of 25 mM Tris HCl buffer and 2 mM sodium dithionite reductant (DT). The samples of apo-NifDK and cofactor are mixed in a water bath at 170 RPM and 30 °C for 30 min. After mixing, the reconstitution mixture is divided into two other vials containing substrate, NifH, ATP-regenerating solution, 25 mM Tris HCl buffer, and 20 mM DT. The hydrocarbon products were analyzed as described elsewhere.[21–23] Ammonium was determined by a high performance liquid chromatography fluorescence method, and hydrogen was analyzed as described previously.[24,25]

4.6 References

(1) Hoover, T. R.; Imperial, J.; Ludden, P. W.; Shah, V. K. *Biochemistry* **1989**, *28* (7), 2768–2771.

(2) Sippel, D.; Einsle, O. *Nat. Chem. Biol.* **2017**, *13* (9), 956–960.

(3) Durrant, M. C.; Francis, A.; Lowe, D. J.; Newton, W. E.; Fisher, K. *Biochem. J.* **2006**, *397* (2), 261–270.

(4) Masukawa, H.; Inoue, K.; Sakurai, H. *Appl. Environ. Microbiol.* **2007**, *73* (23), 7562–7570.

(5) McLean, P. A.; Dixon, R. A. *Nature* **1981**, *292* (5824), 655–656.

(6) Dance, I. *Dalt. Trans.* **2012**, *41* (25), 7647–7659.

(7) Zheng, L.; White, R. H.; Dean, D. R. *J. Bacteriol.* **1997**, *179* (18), 5963–5966.

(8) Hoover, T. R.; Robertson, A. D.; Cerny, R. L.; Hayes, R. N.; Imperial, J.; Shah, V. K.; Ludden, P. W. *Nature* **1987**, *329* (6142), 855–857.

(9) McLean, P. A.; Smith, B. E.; Dixon, R. A. *Biochem. J.* **1983**, *211* (3), 589–597.

(10) Liang, J.; Madden, M.; Shah, V. K.; Burris, R. H. *Biochemistry* **1990**, *29* (37), 8577–8581.

(11) Madden, M. S.; Paustian, T. D.; Ludden, P. W.; Shah, V. K. *J. Bacteriol.* **1991**, *173* (17), 5403–5405.

(12) Fay, A. W.; Blank, M. A.; Lee, C. C.; Hu, Y.; Hodgson, K. O.; Hedman, B.; Ribbe, M. W. *J. Am. Chem. Soc.* **2010**, *132* (36), 12612–12618.

(13) Ribbe, M. W. *Nitrogen fixation : methods and protocols*; Humana, 2011.

(14) Lee, C. C.; Tanifuji, K.; Newcomb, M.; Liedtke, J.; Hu, Y.; Ribbe, M. W. *ChemBioChem* **2018**, *19* (7).

(15) Christiansen, J.; Goodwin, P. J.; Lanzilotta, W. N.; Seefeldt, L. C.; Dean, D. R. *Biochemistry* **1998**, *37* (36), 12611–12623.

(16) Pienkos, P. T.; Shah, V. K.; Brill, W. J. *Proc. Natl. Acad. Sci.* **1977**, *74* (12), 5468–5471.

(17) Lee, C. C.; Hu, Y.; Ribbe, M. W. *Proc. Natl. Acad. Sci.* **2009**, *106* (23), 9209–9214.

(18) Hu, Y.; Fay, A. W.; Dos Santos, P. C.; Naderi, F.; Ribbe, M. W. *J. Biol. Chem.* **2004**, *279* (52), 54963–54971.

(19) Hu, Y.; Corbett, M. C.; Fay, A. W.; Webber, J. A.; Hedman, B.; Hodgson, K. O.; Ribbe, M. W. *Proc. Natl. Acad. Sci.* **2005**, *102* (39), 13825–13830.

(20) Hu, Y.; Fay, A. W.; Schmid, B.; Makar, B.; Ribbe, M. W. *J. Biol. Chem.* **2006**, *281*

(41), 30534–30541.

(21) Lee, C. C.; Hu, Y.; Ribbe, M. W. *Science* **2010**, *329* (5992), 642.

(22) Hu, Y.; Lee, C. C.; Ribbe, M. W. *Science* **2011**, *333* (6043), 753–755.

(23) Sickerman, N. S.; Tanifuji, K.; Lee, C. C.; Ohki, Y.; Tatsumi, K.; Ribbe, M. W.; Hu, Y. *J. Am. Chem. Soc.* **2017**, *139* (2), 603–606.

(24) Corbin, J. L. *Appl. Environ. Microbiol.* **1984**, *47* (5), 1027–1030.

(25) Gavini, N.; Burgess, B. K. *J. Biol. Chem.* **1992**, *267* (29), 21179–21186.

(26) Kowalewski, K.; Gierczak, T. *J. Chromatogr. A* **2011**, *1218* (41), 7264–7274.

(27) Schiller, M.; Von Der Heydt, H.; März, F.; Schmidt, P. C. *J. Chromatogr. A* **2002**, *968* (1–2), 101–111.

Chapter 5:

Characterization of extracted M- and V-clusters within the Δ*nifB* Mo-nitrogenase scaffold

5.1 Abstract

Mo- and V-nitrogenase are two nitrogenase variants present in *Azotobacter vinelandii*. Despite similarities in the structures of their protein scaffolds and catalytic cofactors, V-nitrogenase demonstrates much greater capabilities in terms of converting carbon monoxide (CO) into hydrocarbon products. Attempts to understand the source of reactivity differences between Mo- and V-nitrogenase have primarily focused on characterization of the catalytic M- and V-clusters. Although the cofactor structures play a role in catalytic differences between these two variances, characterizing them in the context of the different Mo- and V-nitrogenase protein scaffolds complicates studies of cofactor characteristics. In this work, the cofactors of Mo- and V-nitrogenase are compared in the context of an apo protein, Δ*nifB* NifDK, to form $NifDK^{M}$ and $NifDK^{V}$. Comparisons of the resulting influence on CO reduction indicates that the protein scaffold of V-nitrogenase is a significant contributor to its CO-reducing capabilities.

5.2 Introduction

Although Mo- and V-nitrogenases can both convert carbon monoxide (CO) into small hydrocarbon products, V-nitrogenase is a better biocatalyst for this conversion.[1,2] In terms of overall CO reduction products, V-nitrogenase generates hydrocarbon products at 16 nanomoles hydrocarbon product per nanomole of catalytic protein per minute of reaction time (nmol/nmol/min) and can produce hydrocarbons as large as butane. The Mo-nitrogenase, on the other hand, produces hydrocarbons as large as propane at ~0.02 nmol/nmol/min. In terms of reaction rate and product size, the V-nitrogenase is roughly 600-fold more efficient at converting CO into hydrocarbon products.[1,2] This capability mirrors Fischer-Tropsch reactivity and represents an exciting opportunity to understand

how biological systems can be used to convert CO pollution in biofuel products. However, the structural features that allow V-nitrogenase to produce hydrocarbon products from CO are not well-understood.

These dissimilarities are especially surprising given the overall structural similarity of the Mo- and V-nitrogenase proteins. The protein scaffolds of Mo- and V-nitrogenase are overall similar in shape, and the primary *α* and *β* subunits of the catalytic components (NifDK and VnfDGK) share ~33% amino acid identity. V-nitrogenase contains a small additional subunit (VnfG, *δ*) with an unknown function. The respective reductase components, NifH and VnfH, share ~91% of amino acid sequence identity.[3] The catalytic cofactors (M- and V-cluster) of both proteins share a similar structure that varies primarily in the terminal metal component (Mo or V) and the apparent structure of the belt-sulfur region of the cofactors. Recent crystal structures of V-nitrogenase revealed that the V-cluster contains a bridging moiety in the belt-sulfur region that appears to be a carbonate group.[4,5] The differences in the protein scaffold and catalytic cofactor of V-nitrogenase raises the question of which of these factors influence the CO reduction capabilities of this variant. An improved understanding of the biochemical factors that lead to the reactivity is an important step towards developing biological or biomimetic systems to convert CO pollution into useful fuel products.

Because both the protein scaffolds and catalytic cofactor structures are different, determining whether once component is more important is challenging. One approach to probe the specific source of these CO reduction capabilities is to create hybrid enzyme systems that utilize different combinations of the Mo- and V-nitrogenase protein scaffolds and catalytic cofactors. This can be accomplished *in vitro* by using extracted V- or M-

cluster samples to reconstitute a cofactor-deficient Mo-nitrogenase (Δ*nifB* NifDK) to form $NifDK^M$ and $NifDK^V$. This method allows for a comparison of the M- and V-cluster reactivity differences in the context of the same protein scaffold. Experiments with $NifDK^M$ and $NifDK^V$ indicated that both hybrids are capable of reducing CO into hydrocarbon products, but the products formed with the reconstituted proteins mirrored those of NifDK rather than VnfDGK. Upon substitution of D_2O for H_2O in the assays reaction buffers, $NifDK^M$ and $NifDK^V$ mirror the reactivity of NifDK. In the presence of D_2O, all three proteins (NifDK, $NifDK^M$, and $NifDK^V$) experience an increased reaction rate and form larger hydrocarbon products.[2,6] Taken together, these results indicate that the protein scaffold of VnfDGK is a large contributor to the CO-reducing capabilities of the enzyme. Additionally, the isotope effect observed in the presence of D_2O indicates that the ability of VnfDGK to form larger hydrocarbon products may stem from its overall slower catalytic rates.

5.3 Results

In these experiments, NifDK and VnfDGK were purified from *A. vinelandii*. The respective catalytic cofactors were extracted from the proteins. The extracted M- and V-cluster were combined with Δ*nifB* NifDK to form $NifDK^M$ and $NifDK^V$. The CO-reducing capabilities of these reconstituted hybrids were compared to the wildtype Mo- and V-nitrogenase enzymes (NifDK and VnfDGK). $NifDK^M$ and $NifDK^V$ were capable of CO reduction (Figure 5.1A). When compared to VnfDGK, neither $NifDK^M$ nor $NifDK^V$ produce detectable amounts of the hydrocarbon products specific to VnfDGK (CH_4, C_4H_8, and C_4H_{10}). Compared to VnfDGK, both $NifDK^M$ and $NifDK^V$ demonstrate rates of hydrocarbon formation that are 640-fold lower than VnfDGK (Figure 5.1B).

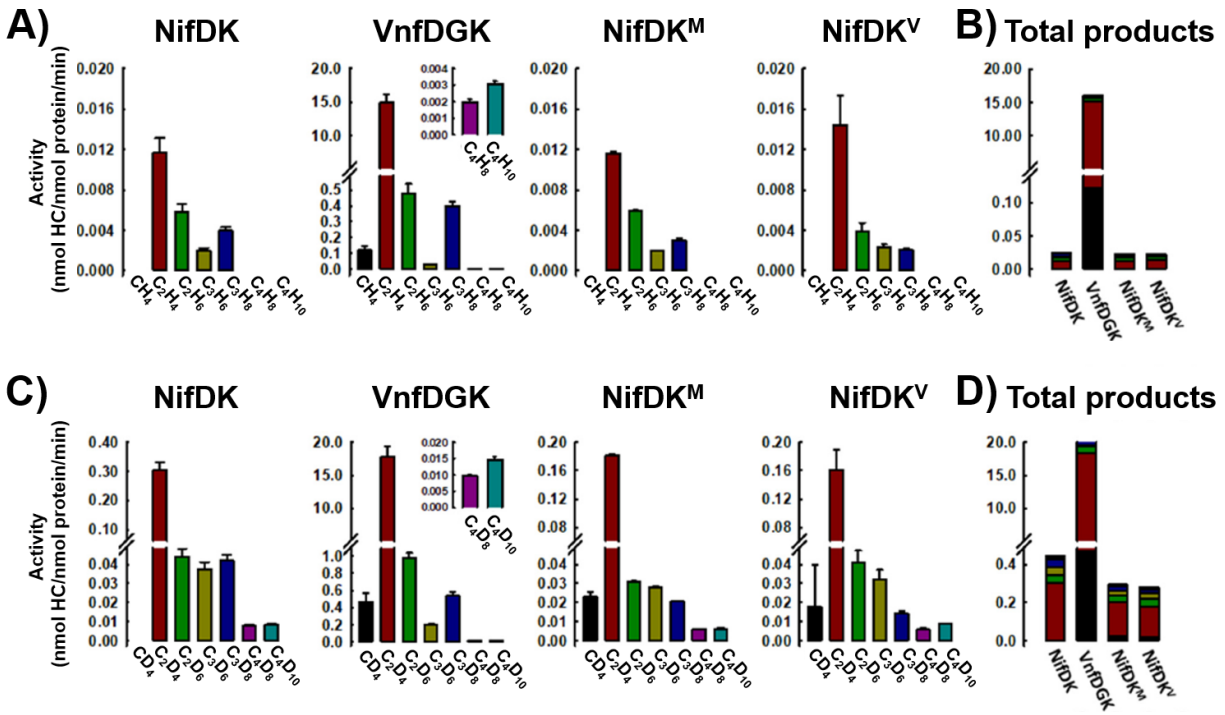

Figure 5.1: Specific activities of hydrocarbon formation from CO reduction by NifDK, VnfDGK, NifDK^M, and NifDK^V in the presence of H_2O (**A**, **B**) and D_2O (**C**, **D**). Shown are bar charts of the individual activities of CH_4, C_2H_4, C_2H_6, C_3H_6, C_3H_8, C_4H_8, and C_4H_{10} formation (**A, C**) and stacked bar charts of the sum of the individual activities (**B, D**) of each protein species. The colors of the stacked bars (**B, D**) correspond to those of the individual bars **(A, C**). Specific activities are expressed as nmol hydrocarbon (HC)/nmol protein/min. Data are presented as mean ± SD (*N* = 4 repetitions of each experiment). Hydrocarbon color codes shown on the right.

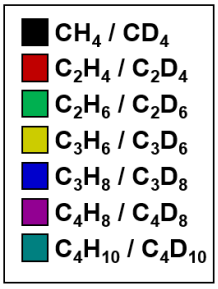

In the presence of D_2O-based reaction buffer, NifDK, NifDK^M, and NifDK^V display the ability to produce C_4H_8 and C_4H_{10} (Figure 5.1C). Additionally, the rate of hydrocarbon production increases 24-fold compared to the rates observed in H_2O-based reaction buffer (Figure 5.1D). In comparison, VnfDGK experiences only a 1.1-fold increase in reaction rate upon exchange of D_2O for H_2O. When the product distributions of NifDK^M and NifDK^V are compared to the native NifDK and VnfDGK proteins, NifDK^V displays a closer resemblance to VnfDGK than NifDK^M. In terms of the production of C_2H_4 from CO,

NifDK^{V} generates ~12% more C_2H_4 than NifDK^{M}, which mirrors the ability of VnfDGK to generate considerably more C_2H_4 than NifDK from CO (Figure 5.2A).

Additionally, upon substitution of D_2O for H_2O, the ~5% reduction in C_2H_4 formation by VnfDGK is paralleled by a ~6% decrease in C_2H_4 formation by NifDK^{V} (Figure 5.2B). NifDK and NifDKM demonstrate a similar relationship. The D_2O-induced ~19% increase of C_2H_4 formation by NifDK is mirrored by a ~10% increase of C_2H_4 formation by NifDK^{M} (Figure 5.2A). These results point to a contribution of the distinct characteristics the cofactor species (M- or V-clusters) in the reactivity nitrogenase variants toward CO.

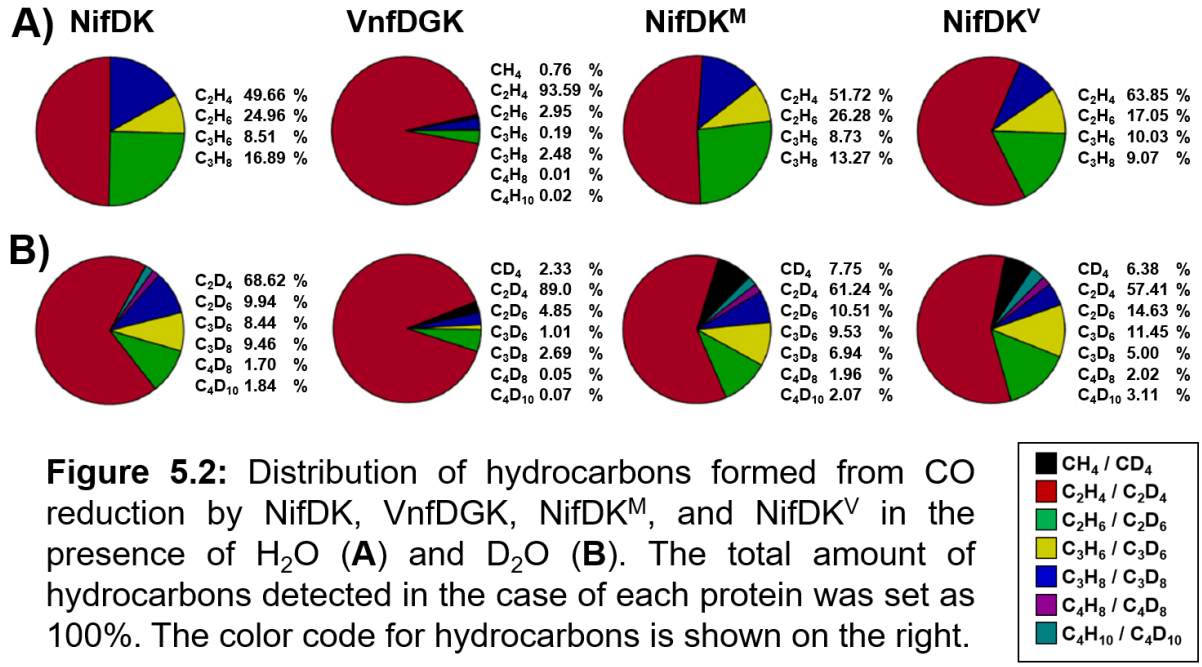

Figure 5.2: Distribution of hydrocarbons formed from CO reduction by NifDK, VnfDGK, NifDK^{M}, and NifDK^{V} in the presence of H_2O (**A**) and D_2O (**B**). The total amount of hydrocarbons detected in the case of each protein was set as 100%. The color code for hydrocarbons is shown on the right.

A detailed examination of the C2 product distributions of NifDK^{M} and NifDK^{V} in D_2O and H_2O supports this perspective. The ratio between the percentages of the unsaturated C2 product (C_2H_4) formed by VnfDGK in D_2O and H_2O is lower than the ratio observed with NifDK (Figure 5.3A). However, the ratio between the percentages of the saturated C2 product (C_2H_6) formed by VnfDGK in D_2O and H_2O is much higher than that of NifDK

(Figure 5.3B). This indicated that C2 product formation is shifted toward the saturated products in the case of VnfDGK upon substitution of D_2O for H_2O. The same trend is observed when $NifDK^V$ and $NifDK^M$ are compared in terms of formation of unsaturated and saturated C2 products in D_2O and H_2O (Figure 5.3B). These influences of product formation indicate that specific features of the V-cluster influence the reactivity of $NifDK^V$ such that the resulting product distribution mirrors that of VnfDGK in this reaction.

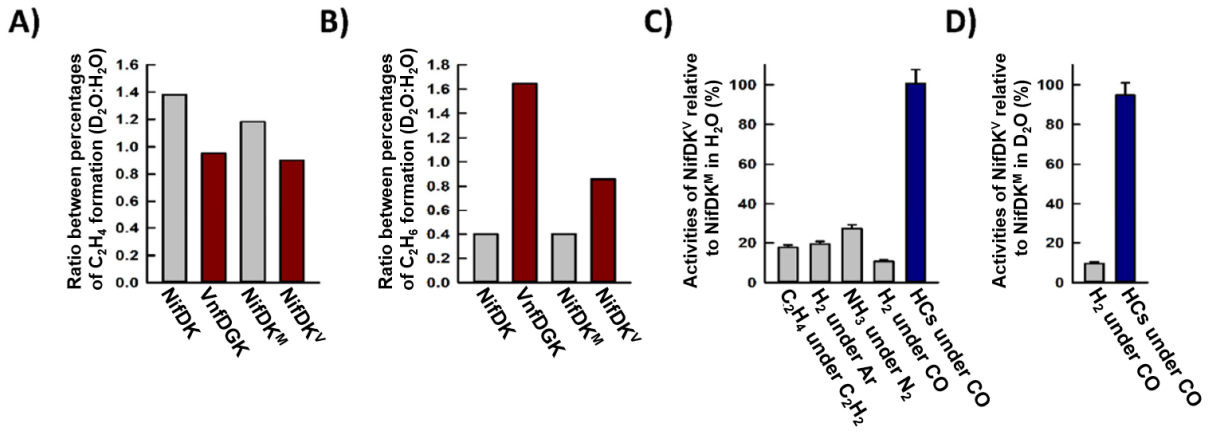

Figure 5.3: Ratios between percentages of C_2H_4 (**A**) and C_2H_6 formation (**B**) in the presence of D_2O and H_2O in reactions catalyzed by NifDK, VnfDGK, $NifDK^M$, and $NifDK^V$; and activities of $NifDK^V$ relative to those of $NifDK^M$ in H_2O (**C**) and D_2O (**D**). The ratios were calculated based on the activities shown in Figure1 (A, B). Activities of C_2H_4 formation under C_2H_2, H_2 formation under Ar, NH_3 formation under N_2, H_2 formation under CO, and hydrocarbon (HCs) formation under CO are shown in **C**. H_2 formation under CO and hydrocarbon formation under CO are shown in **D**. Data in **C** and **D** are presented as mean ± SD (*N* = 4 repetitions of each experiment).

The CO-reducing abilities of VnfDGK are especially interesting given the overall catalytic efficiency of this variant with other substrates. Specifically, when compared to NifDK, VnfDGK demonstrates reduced activity for the reduction of C_2H_2, H^+, and N_2.[1,2,7] Similarly, $NifDK^V$ reduces C_2H_2, H^+, and N_2 at 18%, 19%, and 27%, respectively, of the activities of NifDK (Figure 5.3C). However, with CO as a substrate, $NifDK^V$ generates

hydrocarbons at approximately the same level as $NifDK^M$ in the presence of both H_2O (Figure 5.3C, *blue bar*) and D_2O (Figure 5.3D, *blue bar*). This observation points to CO as a preferred substrate for the V-cluster. In the case of $NifDK^V$, the ability of the V-cluster to reduce CO is inhibited by the seemingly inefficient protein scaffold, NifDK.

5.4 Discussion

Efforts to understand the reactivity and catalytic mechanisms of NifDK and VnfDGK have primarily focused on the active site cofactors.[8,9] In the current study, the reactivity of $NifDK^V$ with CO, as compared to that of $NifDK^M$, showcases a

better efficiency of the V-cluster in CO reduction when compared to the M-cluster.

Such a discrepancy could originate from the presence of different heterometals (*i.e.*, V or Mo) in these clusters, as it has been reported that synthetic vanadium-containing compounds are better than their Mo-counterparts at coupling two CO moieties into functionalized acetylene ligands.[10] On top of a difference in heterometal identity, the recent crystal structures of VnfDGK indicate that the V-cluster contains a carbonate moiety in place of a belt-sulfur atom that would be expected based upon structures of the M-cluster from NifDK.[4,11] This moiety may be a factor in the observed differences between VnfDGK and NifDK, but both the origin and catalytic relevance of this moiety is still unclear at this time.

Although it is evident that some of the catalytic differences between NifDK and VnfDGK stem from the different properties of the M- and V-clusters, this work suggests that the protein scaffold of V-nitrogenase influences reactivity more than expected, especially in the case of CO reduction. Once the extracted cofactors from VnfDGK and

NifDK are placed in a normalized protein environment (Δ*nifB* NifDK), the differences in reactivity that are observed with the intact NifDK and VnfDGK are primarily eliminated. However, the product profile of $NifDK^{V}$ is more similar to that of VnfDGK rather than NifDK. This suggests that the cofactor also plays a role in the increased production of hydrocarbons by VnfDGK, albeit it more minor. These results, in combination with more recently published works with nitrogenase hybrids, indicate that studies of nitrogenase mimics and other biomimetic systems to catalyze the reduction of CO should focus on utilizing unique features of the V-nitrogenase protein scaffold. Additional research is required to elucidate the specific aspects of the protein environment that lead to improved reduction of CO into hydrocarbon products.

5.5 Materials and Methods

5.5.1 Cell growth and protein purification: The *Azotobacter vinelandii* strains were grown in 180-L batches in a 200-L fermenter (New Brunswick Scientific) in Burke's minimal medium supplemented with 2 mM ammonium acetate. Media used for the expression of His-tagged NifDK, non-tagged NifH (in *A. vinelandii* strain YM13A) and His-tagged apo-NifDK (in *A. vinelandii* strain DJ1143) contained 10 μM molybdate as described earlier; and molybdate was replaced by an equal amount of vanadate for the expression of His-tagged VnfDGK and non-tagged VnfH (in *A. vinelandii* strain YM68A).[12–14] Cell growth was monitored by measuring the cell density at 436 nm using a Spectronic 20 Genesys spectrophotometer. Cells were harvested in the late exponential phase by a flow-through centrifugal harvester (Cepa), and the cell paste was washed with a buffer containing 50 mM Tris-HCl (pH 8.0). Published methods were used for the purification of His-tagged NifDK, apo-NifDK, VnfDGK, and non-tagged NifH and VnfH.[12–14]

5.5.2 Cofactor extraction and reconstitution of apo-NifDK: The NifDK- and VnfDGK-bound M- and V-clusters were extracted into *N*-methylformamide (NMF), respectively, using a previously established method.[15] The extracted M- or V-cluster was then incubated with apo-NifDK for 20 min prior to the removal of excess metal clusters via a single passage of the reconstituted protein through a G25 column.

5.5.3 Activity assays: All nitrogenase activity assays were carried out as described earlier.[16,17] The hydrocarbon products were analyzed as described elsewhere.[1,2] Ammonium was determined by a high-performance liquid chromatography fluorescence method, and hydrogen was analyzed as described previously.[18,19]

5.6 References

(1) Lee, C. C.; Hu, Y.; Ribbe, M. W. *Science* **2010**, *329* (5992), 642.

(2) Hu, Y.; Lee, C. C.; Ribbe, M. W. *Science* **2011**, *333* (6043), 753–755.

(3) Hu, Y.; Lee, C. C.; Ribbe, M. W. *Dalt. Trans.* **2012**, *41* (4), 1118–1127.

(4) Sippel, D.; Einsle, O. *Nat. Chem. Biol.* **2017**, *13* (9), 956–960.

(5) Sippel, D.; Rohde, M.; Netzer, J.; Trncik, C.; Gies, J.; Grunau, K.; Djurdjevic, I.; Decamps, L.; Andrade, S. L. A.; Einsle, O. *Science* **2018**, *359* (6383), 1484–1489.

(6) Lee, C. C.; Hu, Y.; Ribbe, M. W. *Angew. Chem. Int. Ed.* **2011**, *50* (24), 5545–5547.

(7) Eady, R. R. *Chem. Rev.* **1996**, *96* (7), 3013–3030.

(8) Hoffman, B. M.; Lukoyanov, D.; Yang, Z. Y.; Dean, D. R.; Seefeldt, L. C. *Chem. Rev.* **2014**, *114* (8), 4041–4062.

(9) Bjornsson, R.; Neese, F.; DeBeer, S. *Inorg. Chem.* **2017**, *56* (3), 1470–1477.

(10) Carnahan, E. M.; Protasiewicz, J. D.; Lippard, S. J. *Acc. Chem. Res.* **1993**, *26* (3), 90–97.

(11) Spatzal, T.; Aksoyoglu, M.; Zhang, L.; Andrade, S. L. a.; Schleicher, E.; Weber, S.; Rees, D. C.; Einsle, O. *Science* **2011**, *334* (6058), 940–940.

(12) Lee, C. C.; Hu, Y.; Ribbe, M. W. *Proc. Natl. Acad. Sci.* **2009**, *106* (23), 9209–9214.

(13) Hu, Y.; Fay, A. W.; Schmid, B.; Makar, B.; Ribbe, M. W. *J. Biol. Chem.* **2006**, *281* (41), 30534–30541.

(14) Ribbe, M. W.; Hu, Y.; Guo, M.; Schmid, B.; Burgess, B. K. *J. Biol. Chem.* **2002**, *277* (26), 23469–23476.

(15) Fay, A. W.; Blank, M. A.; Lee, C. C.; Hu, Y.; Hodgson, K. O.; Hedman, B.; Ribbe, M. W. *J. Am. Chem. Soc.* **2010**, *132* (36), 12612–12618.

(16) Hu, Y.; Fay, A. W.; Dos Santos, P. C.; Naderi, F.; Ribbe, M. W. *J. Biol. Chem.* **2004**, *279* (52), 54963–54971.

(17) Burgess, B. K.; Jacobs, D. B.; Stiefel, E. I. *Biochim. Biophys. Acta* **1980**, *614* (1), 196–209.

(18) Gavini, N.; Burgess, B. K. *J. Biol. Chem.* **1992**, *267* (29), 21179–21186.

(19) Corbin, J. L. *Appl. Environ. Microbiol.* **1984**, *47* (5), 1027–1030.